Journal of Power Sources 240 (2013) 66–79

Contents lists available at SciVerse ScienceDirect

Journal of Power Sources

journal homepage: www.elsevier.com/locate/jpowsour

Review

Graphene in lithium ion battery cathode materials: A review

Gints Kucinskis*, Gunars Bajars, Janis Kleperis

Institute of Solid State Physics, University of Latvia, 8 Kengaraga Street, LV-1063 Riga, Latvia

HIGHLIGHTS

- The use of graphene in lithium ion battery cathode materials has been reviewed.
- Graphene improves electron conductivity of lithium ion battery cathode materials.
- Graphene nanosheets form an electron conducting network within the cathode.
- Graphene composite cathodes have superior rate capability and cyclability.

GRAPHICAL ABSTRACT

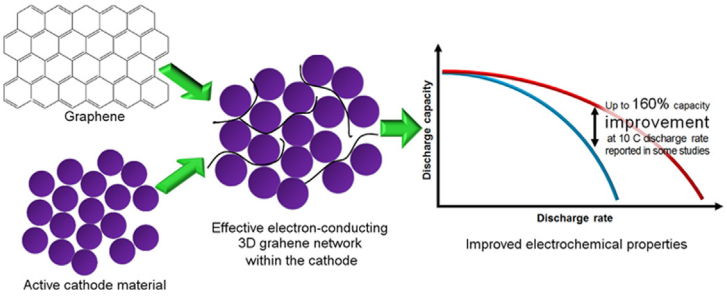

ARTICLE INFO

Article history:
Received 31 December 2012
Received in revised form
25 March 2013
Accepted 27 March 2013
Available online 26 April 2013

Keywords:
Lithium ion battery
Cathode materials
Graphene
Rate capability
Review

ABSTRACT

Graphene is a relatively new and promising material, displaying a unique array of physical and chemical properties. Although considered to be especially promising for the use in energy storage applications, graphene has only recently been implemented as an electron conducting additive for lithium ion battery cathode materials. In current studies graphene is found to significantly improve cathode electrochemical performance. As the charge capacity, rate capability and cyclability of lithium ion batteries are still in ever-remaining need of improvement, this article examines the prospects of graphene implementation into lithium ion battery cathodes to meet such demands. The existing literature and recent advances on the topic have been reviewed, covering the preparation of graphene and graphene composite lithium ion battery cathodes, their structure and electrochemical properties along with underlying principles for electrochemical performance enhancement of such materials.

1. Introduction

Lithium ion battery, first introduced to market in 1991 by Sony [1] and largely made possible by the early research of Mizushima et al. [1–3], is currently one of the most popular battery technologies in the world. Although widely used in various portable electronic devices [4], only recently have lithium ion batteries entered into the commercial electric vehicle market. Some still question the viability of the technology to meet the needs of consumers' lifestyles [5].

The key parameters for lithium ion batteries are energy and power density (both gravimetric and volumetric), cyclability, rate capability, safety, dependence from temperature and the cost of production. Many of the electrochemical properties of battery materials are directly connected with the conductivity, both electronic and ionic [6]. It is also true in the case of the cathode material, the heaviest and second most expensive component of lithium ion battery [5]. Conductivity and other electrochemical properties of a cathode material can usually be modified through doping [7,8] modifying particle size or shape [9,10] and by using conductive additives, mostly consisting of carbon: carbon black,

* Corresponding author.
E-mail addresses: gints.kucinskis@gmail.com (G. Kucinskis), gunars.bajars@gmail.com (G. Bajars), kleperis@latnet.lv (J. Kleperis).

0378-7753/$ – see front matter © 2013 Elsevier B.V. All rights reserved.
http://dx.doi.org/10.1016/j.jpowsour.2013.03.160

carbon coatings [8,11], conducting polymers, for instance polypyrrole (PPy) or polyethylene glycol (PEG) [12], carbon nanotubes [13,14], etc. It has recently been shown that graphene can be used as a conducting additive and in many cases is displaying remarkable results [15–34].

Conventional carbon additives such as carbon black and carbon coatings possess relatively low electronic conductivities when compared with more crystalline forms of carbon. Crystallization of conductive additives within the material itself is rendered impossible due to the rather low melting temperatures of active cathode materials. Since in the case of carbon black only the outer surface is in contact with the active material and only outer layers contribute to the electrical conductivity of the material [35], carbon materials with larger surface/mass ratios are researched. Graphene has an extremely high surface/mass ratio, and sp^2 bonded carbon atoms arranged in hexagonal 2D lattice ensure one of the highest electron conductivities [36]. Therefore graphene could be an exceptionably suitable candidate for the use in lithium ion battery cathodes as an electron conducting additive.

Owing to the relatively recent research advancements regarding graphene, especially by A. Geim and K. Novoselov [37], which have been awarded with a Nobel Prize in Physics in 2010 "for groundbreaking experiments regarding the two-dimensional material graphene", the number of papers studying graphene has grown significantly [38]. The prospect of using graphene in energy harvesting and storage devices is being considered particularly interesting [39]. Underlying reasons for that are several unique properties of the material, such as high charge carrier mobility (20 $m^2 V^{-1} s^{-1}$) [40], high theoretical surface area of 2630 $m^2 g^{-1}$ [41] and a broad electrochemical window [42]. Regarding the energy production and storage applications, graphene has mostly been studied for use in solar cells [43–45], fuel cells [46–48], supercapacitors [49–51], lithium-air batteries [52–54] and lithium ion batteries (as an additive to both anode [55–57] and cathode [15–35]).

Although several review articles are available about graphene and its composites in energy storage devices [39,58–60], little attention has been devoted to graphene in lithium ion battery cathode materials. As there are already numerous studies [15–35] and several patents [61–63] regarding the use of graphene in lithium ion battery cathode materials, this review article attempts to summarize those studies, draw conclusions on the underlying physicochemical mechanisms and explore further research possibilities.

2. Overview

2.1. Lithium ion battery cathode materials

Some of the most commonly studied cathode materials for lithium ion batteries are $LiCoO_2$, $LiMn_2O_4$ and $LiFePO_4$. These have electronic conductivities of 10^{-4} S cm^{-1} [64–66], 10^{-6} S cm^{-1} [67,68] and 10^{-9} S cm^{-1} [69,70] respectively. Another perspective cathode material is $Li_3V_2(PO_4)_3$, which has an electronic conductivity of 2.4×10^{-7} S cm^{-1} [71]. These are fairly low values and can often impair cathode rate capability, thus frequently electron conducting additives are added to such materials in order to improve their electrochemical properties.

As $LiFePO_4$ has a particularly low electronic conductivity, it is only reasonable that most of the graphene research as an electron conducting additive for lithium ion battery cathode materials is currently directed toward $LiFePO_4$/graphene materials [15–25,35]. However, there are also several studies on $LiMn_{1-x}Fe_xPO_4$/graphene [26], $LiMn_2O_4$/graphene [27–29] and $Li_3V_2(PO_4)_3$/graphene [30–34] composites. To the best of our knowledge, however, there are currently no published studies specifically on $LiCoO_2$/graphene composites.

$LiFePO_4$ is a lithium ion battery cathode material with an olivine-type structure, where phosphorus occupies tetrahedral sites, transition metal occupies octahedral sites and lithium ions form one-dimensional chains along the [010] direction [72]. Lithium ion intercalation and de-intercalation takes place via one-dimensional channels [72]. Although some commonly used lithium metal oxides can offer better charge capacities [73], $LiFePO_4$ is generally regarded as a perspective cathode material due to its low production costs and superior cyclability [74]. $LiFePO_4$ has already been implemented in numerous commercial batteries, some of them focusing on automotive market [75]. Thin films of $LiFePO_4$ have also been researched [76–78]. $LiFePO_4$ has a low conductivity of both electrons and lithium ions. These low conductivities are considered to be the main drawbacks of the material, limiting rate capability and, to some extent, also cyclability. There have been numerous attempts of improving its rate capability by modifying grain shape and size, doping and adding electrically conductive additives [79–83]. As shown further, some experimental works with graphene as a conductive additive offer a superior rate capability to those achieved by other methods.

$Li_3V_2(PO_4)_3$ is another phosphate material researched for use as a cathode in lithium ion batteries. Contrary to $LiFePO_4$, it has a monoclinic structure [84]. Its higher operating voltage and high rate capability make it a promising cathode material [85,86].

$LiMn_2O_4$ forms a spinel structure, in which manganese is located in the octahedral sites and lithium occupies the tetrahedral sites [87]. Lithium intercalation and de-intercalation takes place in three-dimensional network of channels rather than planes. Although its cost of production is relatively low [88], it also has a fairly low charge capacity when compared to other popular cathode materials [67], and phase changes during cycling might take place [89]. Mn^{2+} dissolution into the electrolyte can also be a problem [90]. Other transition metals (most often nickel, cobalt and iron) can be added to $LiMn_2O_4$ in order to improve its electrochemical performance [91–93].

2.2. Graphene and graphene oxide

Graphene is a monolayer of graphite, consisting of sp^2 hybridized carbon atoms arranged in a honeycomb crystal lattice. It is a two-dimensional material, meaning that every atom of graphene can be considered as a surface atom. Graphene forms a basic structure of other carbon materials like graphite, carbon nanotubes and fullerenes. Graphene possesses a highly unique electronic structure because of the charge carriers behaving like relativistic particles [37,94], thus unusual phenomena, such as anomalous quantum Hall effect [37,95], exist in graphene. The ballistic charge transport at room temperature and at high charge carrier concentrations make graphene interesting for applications where electronic conductivity is of high importance [96].

Graphene can be prepared in various ways: micromechanical exfoliation of highly oriented pyrolytic graphite with or without previous processing of the surface [37,97,98], epitaxial growth [99,100], chemical vapor deposition (CVD) [101,102] and reduction of graphene oxide (GO) [103–107]. From the aforementioned methods the most suitable for large-scale graphene production is the reduction of GO [108]. It must also be noted that the vast majority of graphene composite lithium ion battery cathode materials use graphene obtained by reducing GO [15–17,19–23,26,28,30–34].

Despite the novelty of graphene, some parts of the research have a history dating back to more than one and a half century, when the earliest paper discussing oxidation of graphite was

published by B.C. Brodie in 1859 [109]. Currently one of the most popular is the method first reported by Hummers and Offerman in 1958 [110], where graphite oxide (oxidized graphite) has been prepared by treating graphite with a mixture of three oxidizing agents – sulfuric acid (H_2SO_4), sodium nitrate ($NaNO_3$) and potassium permanganate ($KMnO_4$). It is then rinsed with water and hydrogen peroxide and filtered afterward. After that resinous anion and cation exchangers are used to remove the remaining impurities. Although graphite oxide retains the stacked layer structure of graphite, it incorporates oxygen and hydrogen containing groups. These groups increase the interlayer distance and due to weakening of the platelet–platelet interactions make the atom-thick graphite oxide layers hydrophilic [108]. One or few monolayers of graphite oxide are called graphene oxide (GO). A variety of thermal and mechanical methods can be used to exfoliate graphite oxide to graphene oxide, although sonicating and/or stirring GO in water are the most common [111].

During the last years modifications of the Hummers method have been proposed and implemented by some authors [22,26,32,112–117]. N.I. Kovtyukhova et al., for instance, proposed an additional oxidation step prior to the oxidation of graphite by Hummers' method [112]. This reportedly helped to avoid incompletely oxidized graphite-core/GO-shell particles in the final product. Pre-oxidizing was accomplished by treating graphite powder in 80 °C hot solution of concentrated H_2SO_4, $K_2S_2O_8$ and P_2O_5 for 6 h and then diluting, washing and filtering the mixture until the rinse water pH becomes neutral. After that the graphite oxide preparation preceded with Hummers method. A more recent improvement of the original Hummers method has been proposed by D.C. Marcano and colleagues [113], who found that excluding $NaNO_3$, increasing the amount of $KMnO_4$ and performing the reaction in a mixture of H_2SO_4/H_3PO_4 (9:1) improves the efficiency of the graphite oxidation process. Some less altered modifications of Hummers method have also been used; in most of these the main difference lies in the graphene to oxidants mass ratio used or oxidation times [22,26,114,115].

Due to its complexity and partial amorphous characteristics, the precise chemical structure of both graphite oxide and GO is yet to be fully understood [111]. Several models exist, most widely accepted, however, is the one proposed by Lerf and Klinowski [118,119] (see Fig. 1). By using solid state nuclear magnetic resonance (NMR) spectroscopy to characterize the material, A. Lerf, J. Klinowski and colleagues were able to propose a nonstoichiometric model, containing hydroxyl and epoxy functional groups as well as some carbonyl groups (carboxyl, carbonyl, ester) along the GO sheet edge. Their studies as well as studies by other authors also suggested a presence of esters and tertiary alcohols on the surface [118–121]. It must, however, be noted, that several other models exist, including a model proposed by Dekany and coworkers [122], which suggests a regular, corrugated quinoidal structure interrupted by trans-linked cyclohexyl regions, functionalized by tertiary alcohols and 1,3-ethers [111].

The conductivity of graphene relies mainly on the long-range conjugated network of graphitic lattice. Both graphite oxide and graphene oxide (GO) are electrically insulating materials due to their disrupted sp^2 bonding networks [123]. Functionalization present in GO breaks the conjugated structure and localizes π-electrons, resulting in a decrease of both carrier mobility and carrier concentration [108,111]. Reduction of GO results in a partial restoration of the electrical conductivity by restoring the π-network. The material obtained by reducing GO is generally referred to as reduced graphene oxide (rGO) or simply graphene. As most of the graphene materials in studies reviewed here are obtained by reducing GO, it will be called graphene or graphene nanosheets further in the text.

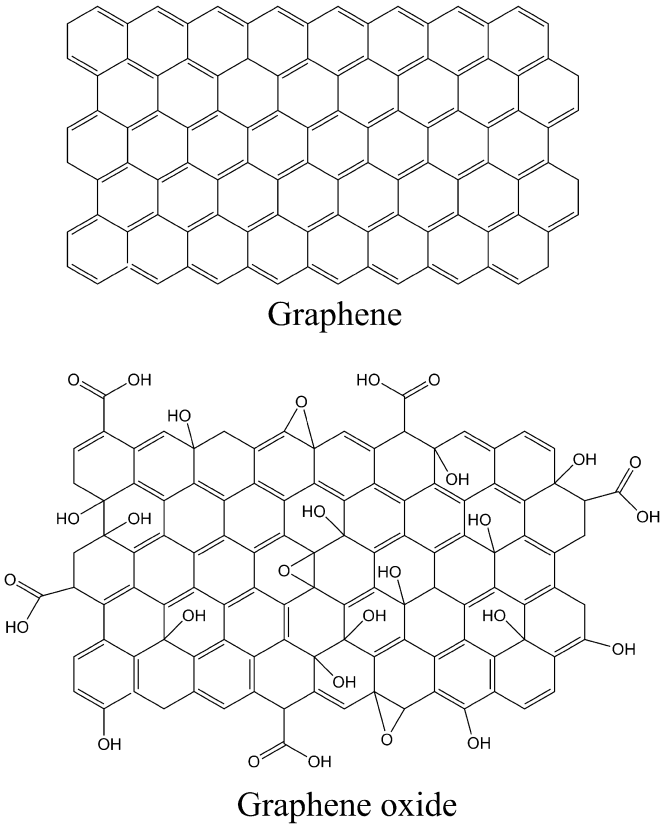

Fig. 1. The structural model of graphene and variations of the atomic structure of GO with carboxyl groups at the sides as proposed by Lerf and Klinowski [118].

GO can be reduced thermally, chemically, electrochemically or by using combinations of several aforementioned methods. Chemical reduction is the most common [111]. In chemical reduction reducing compounds are used to strip away the oxide functionality from the surface. As a direct consequence to the hydrophilic character of graphite oxide, GO is usually processed in water. Thus it is very convenient, if the GO nanolayers obtained can be reduced while the water is still present. Such chemical reduction requires reducing compounds that would not react with water. One of such compounds is hydrazine and its derivatives (hydrazine monohydrate, dimethylhydrazine). Although hydrazine is considered to be highly toxic, its strong reducing properties as well as non-reactivity with water make it one of the most studied reagents for the reduction of GO. The exact reduction mechanism is still largely unknown, but there have been many characterizations of hydrazine reduced GO [103–107]. One of the highest conductivities of reduced GO films produced solely by hydrazine reduction is 99.6 S cm^{-1} with a C/O ratio of around 12.5 [107]. $NaBH_4$ has been demonstrated to be a more efficient reductant of GO than hydrazine [124]. Although it is hydrolyzed by water, the process is slow enough for $NaBH_4$ to reduce GO first. Recently Ascorbic acid (Vitamin C) has been demonstrated to be a good substitute for hydrazine [107]. Hydroiodic acid [125] and oxalic acid [126] have also been reported as good reductants. TiO_2 is reported to function as a reductant in a photocatalytic GO reduction under ultraviolet (UV) irradiation [127]. Electrochemical GO reduction is also possible [128]. It is carried out in an electrochemical cell with a GO electrode and an aqueous buffer solution. After depositing GO thin film on a substrate (ITO, glass, plastic, etc.), an inert electrode is used as a counter electrode in the electrochemical cell [108]. However, electrochemical processes can also be used to obtain

graphene directly from electrochemically exfoliated graphite [29,129]. In this case no graphite oxide or GO phases are necessary.

Thermal treatment has been used for graphite oxide exfoliation and GO reduction in several experiments [130–132] and can be carried out in vacuum, inert or reducing atmospheres. When graphite oxide is subjected to high temperature heating, the high temperature forces the oxygen-containing functional groups attached to the carbon plane to decompose into gas phase (mostly CO_2) that create huge pressure between the stacked layers [130,133]. However, this can only happen if the diffusion of the evolved gases is sufficiently small to secure the rise of pressure and therefore graphite oxide exfoliation and formation of single sheet GO [133]. Based on the state equation [134], a pressure of 40 MPa is generated at 200 °C, and a pressure of 130 MPa is generated at 1000 °C [133]. Evaluation of Hamaker constant predicts that a pressure of only 2.5 MPa is enough to separate two stacked GO platelets [133]. It is suggested from theoretical studies that critical temperature of 550 °C should be exceeded for graphene exfoliation to occur [133].

It has been found that the thermal treatment can not only exfoliate graphite oxide, thus resulting in preparation of GO, but also strip away some oxide functionalities from the surface of GO [131–133,135], efficiently meaning that graphene can be obtained directly by thermal exfoliation of graphite oxide. Thermal reduction can be used to reduce GO that has been obtained by other methods (e.g. by dispersing graphite oxide in water) [131,132]. Unsurprisingly, experimental evidence suggests that the structure of reduced GO is temperature-dependent [135]. Aside from the reduction of GO, thermal treatment is also found to remove chemical contaminants that can adhere to the graphene during processing and degrade its electronic properties [136].

It has been found that thermal reduction of GO can only produce small and wrinkled graphene sheets [130]. Around 30% of the mass of the GO is lost during the exfoliation process, the loss is attributed to mostly CO_2 [130,133], possibly creating lattice defects throughout the sheet. The oxygen-containing groups remove carbon atoms from the carbon plane, thus splitting graphene sheets into smaller pieces and resulting in the distortion of the carbon plane [130]. Some of the defects induced by thermal reduction can be avoided if the procedure is carried out after the formation of bulk materials (thin films, powders, etc.) by annealing in inert or reducing atmospheres [137]. In such processes temperature is of high significance, with some researchers reporting higher temperatures consequently yielding improved graphene electron conductivities, when treated in reducing (Ar/H_2) atmosphere [131]. However, when heat-treated in air, sharp decrease in conductivity is observed at temperatures above 350 °C [138]. Conductivity of the reduced GO also depends on the duration of the thermal treatment [139].

Thermal and chemical GO reduction methods can be combined in order to obtain better conducting rGO. Results obtained with the density functional theory (DFT) method suggest that some of the functional groups attached to graphene lattice can be removed only by chemical reduction, whereas some – only by thermal annealing [140]. For more information on GO chemistry and reduction methods readers can be redirected to review articles dedicated exclusively for such topics [94,108,111].

3. Cathode preparation and structural characterization

3.1. Preparation

Graphene used in most of the works regarding graphene composite cathodes has been acquired by reducing GO [15–17,19–23,26–28,30–34]. GO is usually prepared by a method developed by Hummers and Offeman [110] or by some variations of it [22,26,32,112–117,141] as discussed in previous section. As GO is considered to be an insulator due to disrupted carbon sp^2 bonding networks [111], a reduction of the material is needed. Various authors use different methods, which are summarized in Table 1. The reduction is often chemical, thermal or a combination of both. More often at least a part of GO reduction is carried out with GO mixed with the precursor. Often GO nanosheets are used instead of graphene, as GO is highly hydrophilic and thus it is easier mixed with the nanoparticles of the cathode material [21]. It is also known that reduction of GO, when being part of a bulk material, enables the exfoliation of graphene sheets with larger lateral sizes [137,142].

Mostly GO or graphene nanosheets are mixed with the precursor of the cathode material. After the precursor is mixed with graphene, conventional methods are used for graphene containing cathode material synthesis. Conventional synthesis methods often include heating in temperatures as high as 750 °C, often in reducing Ar/H_2 (95:5) atmosphere, thus synthesis of cathode material and reduction of GO take place simultaneously. $LiFePO_4$/graphene nanocomposites have been acquired by various synthesis routes, most popular being hydrothermal [20,21], solvothermal [15,17] and solid state [18,19,23] routes. There has also been a study with sol–gel synthesis [16]. More unconventional routes have been taken by Y. Ding et al. and O. Topracki et al., who have prepared $LiFePO_4$/graphene nanocomposites with co-precipitation and electrospinning methods respectively [22,24]. It must also be noted that some of the studies involve more complicated structures, such as microporous $LiFePO_4$/graphene composite [16], graphene encapsulated $LiFePO_4$ [19], $LiFePO_4$ particles encapsulated in graphene containing carbon nanofibers [24] and $LiMn_{1-x}Fe_xPO_4$ nanorods [26]. $Li_3V_2(PO_4)_3$/graphene cathode has been prepared by using sol–gel [30,32,34], solid state [33] and spray-drying [31] synthesis methods. The preparation of $LiMn_2O_4$/graphene composites is slightly different. Two step syntheses have been implemented – first manganese oxide/graphene composites are prepared (MnO_2/graphene [27,28] or Mn_2O_3/graphene [29]), after which they are lithiated.

GO is often ultrasonicated and stirred before reduction. However, it is known that sonicating in water or polar organic media, despite being a much faster method than mechanical stirring, causes substantial damage to the graphene oxide platelets [143]. The dimensions are reduced to only few hundred nanometers per side and the product contains considerably larger distribution of sizes [111,123]. Most works manage to obtain graphene nanosheets with a thickness of 2–3 layers of graphene [18,29].

Interestingly, studies by Y. Tang et al. [18] and X. Zhou et al. [21] are the only ones where graphene has been added after the $LiFePO_4$ synthesis (it must be noted, however, that Y. Zhou and coworkers have performed an extensive mixing of the particles and carried out an additional heat treatment [21]). The ground for mixing graphene with $LiFePO_4$ precursors instead of as-prepared $LiFePO_4$ is the attempt of making a better dispersed and more homogenous electron conducting net of graphene throughout the sample. It is also considered that graphene can reduce the grain size during the synthesis [22]. However, from the experimental studies [18,21] no direct evidence can be collected that such steps would make significant difference in terms of electrochemical properties (see Table 1 and further paragraphs).

3.2. Structure

Common non-electrochemical methods for lithium ion battery material characterization are Raman spectroscopy, X-ray diffraction (XRD) analysis, scanning electron microscopy (SEM) and transmission electron microscopy (TEM). BET analysis (named after S.

Table 1
Preparation of lithium ion battery cathode materials containing graphene.

Cathode material	Preparation of graphite oxide	Reduction of GO	Synthesis	Composite structural model (see Fig. 3)	Ref.
$LiFePO_4$	Hummers method	Chemical (hydrazine monohydrate), thermal	GO ultrasonicated in water, reduced by hydrazine at 100 °C, mixed with precursor, autoclaved (solvothermal synthesis), mixed with sucrose in water, dried, then calcinated at 650 °C (N_2)	Mixed	[15]
$LiFePO_4$	Hummers method	Thermal	Thermally exfoliated graphite oxide ultrasonicated in water, mixed with precursor (sol–gel synthesis), dried, calcinated at 700 °C (Ar)	Mixed	[16]
$LiFePO_4$	Modified Hummers method	Chemical (hydrazine monohydrate, citric acid), thermal	GO ultrasonicated, reduced by hydrazine, mixed with precursor in ethylene glycol, autoclaved (solvothermal synthesis), dried, mixed and ground with citric acid, acetone added, calcinated at 600 °C (Ar/H_2 95:5)	Mixed	[17]
$LiFePO_4$	Graphene deposited on a porous nickel substrate via a CVD method, followed by dissolution of nickel in HCl		$LiFePO_4$ (solid state synthesis) mixed with graphene in *N*-methyl pyrrolidinone (NMP), stirred, NMP evaporated at 80 °C	Mixed	[18]
$LiFePO_4$	Modified Hummers method[a] [114]	Thermal	GO encapsulated FeOOH as a part of precursor also containing polyethylene glycol (PEG), milled in ethanol, dried, calcinated at 700 °C	Encapsulated	[19]
$LiFePO_4$	Hummers method	Chemical (ascorbic acid), thermal	Precursor containing ascorbic acid dispersed in water and mixed with graphite oxide, autoclaved, dried (hydrothermal synthesis), calcinated at 600 °C (Ar/H_2 95:5)	Anchored/wrapped/ mixed	[20]
$LiFePO_4$	Modified Hummers method[a,c] [21]	Thermal	$LiFePO_4$ (hydrothermal synthesis) and GO mixed in water, stirred, ultrasonicated, spray dried at 200 °C, heated at 600 °C (Ar)	Encapsulated (loosely)/mixed	[21]
$LiFePO_4$	Modified Hummers method[a,c] [22]	Chemical (hydrazine monohydrate), thermal	GO ultrasonicated in water, reduced by hydrazine at 100 °C, mixed with precursor (co-precipitation method), heated to 120 °C, sintered at 700 °C (Ar)	Anchored/mixed	[22]
$LiFePO_4$	Hummers method	Thermal	Precursor (solid state synthesis) ball milled, mixed with GO, ultrasonicated in ethanol, dried, heated at 350 °C (N_2), sintered at 700 °C (N_2)	Mixed	[23]
$LiFePO_4$	Commercially available graphene flakes (conductivity – 10^5 S m^{-1})		Precursor and polyacrylonitrile (PAN) mixed with graphene flakes in *N*,*N*-dimethylformamide (DMF), electrospun, stabilized at 280 °C, calcinated at 700 °C (Ar)	Mixed	[24]
$LiFePO_4$	Vacuum-promoted low-temperature approach[142]		Graphene heat-treated in 500 °C, $LiFePO_4$ mixed with graphene and PVDF (polyvinylidene fluoride) in ethanol, spread on aluminum current collector (a step for electrochemical test cell preparation), dried.	Mixed	[25]
$LiMn_{1-x}Fe_xPO_4$	Modified Hummers method[a] [115]	Chemical (ascorbic acid)	Fe doped Mn_3O_4 nanorods prepared on low oxygen content GO sheets (hydrolysis), solvothermal reaction with Li^+ and PO_4^{3-} ions with ascorbic acid present in the solution	Anchored	[26]
$LiMn_2O_4$	–		MnO_2/rGO composite prepared via redox reaction between rGO and MnO_4^- in aqueous solution, followed by a reaction with LiOH	Anchored	[27]
$LiMn_2O_4$	Modified Hummers method	Chemical (hydrazine monohydrate)	GO reduced by hydrazine in hydrazine hydrate, sonicated in water, MnO_2/rGO composite prepared in aqueous solution, dried, lithiated by using microwave-assisted hydrothermal (MAH) conditions at 200 °C	Anchored	[28]
$LiMn_2O_4$	Mn_3O_4/graphene composite prepared by electrolysis of $MnSO_4$ by using graphite sheets as electrodes (electrochemical graphene exfoliation), lithiated via molten salt process			Anchored/mixed	[29]
$Li_3V_2(PO_4)_3$	Modified Hummers method[a,b,c] [116]	Thermal	Sol–gel synthesis precursor mixed with GO, stirred, dried, heated at 350 °C (Ar), ball milled, calcinated at 750 °C (Ar/H_2 95:5)	Anchored/mixed	[30]
$Li_3V_2(PO_4)_3$	Modified Hummers method[a,b,c] [117]	Chemical (citric acid), thermal	GO mixed with $Li_3V_2(PO_4)_3$ precursor containing citric acid, stirred, spray dried at 200 °C, heated to 300 °C (N_2), then heated to 700 °C (N_2)	Anchored/mixed	[31]

Table 1 (*continued*)

Cathode material	Preparation of graphite oxide	Reduction of GO	Synthesis	Composite structural model (see Fig. 3)	Ref.
$Li_3V_2(PO_4)_3$	Modified Hummers method[a] [32]	Chemical (ascorbic acid, oxalic acid), thermal	GO ultrasonicated in ascorbic acid solution, mixed with the sol–gel synthesis precursor containing oxalic acid, ultrasonicated at 80 °C, dried, heated at 350 °C (N_2) followed by calcination at 800 °C (N_2)	Anchored/ wrapped	[32]
$Li_3V_2(PO_4)_3$	Modified Hummers method[a,b,c] [117]	Thermal	Solid state synthesis precursor mixed with GO, ball milled, dried, preheated at 350 °C (Ar), grounded, sintered at 750 °C (Ar/H_2)	Anchored/ wrapped	[33]
$Li_3V_2(PO_4)_3$	Modified Hummers method[a,c] [34]	Chemical (ascorbic acid, oxalic acid), thermal	GO partially reduced by ascorbic acid, mixed with sol–gel synthesis precursor containing oxalic acid, ultrasonicated at 80 °C, dried, heated at 350 °C (N_2) followed by calcination at 800 °C (N_2)	Anchored/ wrapped	[34]

[a] Hummers method modified by changing oxidants – graphite mass ratio.
[b] Hummers method modified according to Kovtyukhova et al. [112].
[c] Hummers method modified by excluding $NaNO_3$ from the reaction.

Brunauer, P. H. Emmett, and E. Teller), which quantifies the surface area of the material by measuring the amount of gas physisorbed to the surface [144], can be implemented. Sometimes X-ray photoelectron spectroscopy (XPS) [17] and extended X-ray absorption fine structure (EXAFS) spectroscopy [28] are used. Similarly, for graphene composite cathode materials Raman spectroscopy, XRD analysis, SEM, TEM and BET analysis are used. Essential for rGO, however, is also the electronic conductivity and carbon to oxygen atomic ratio (C/O ratio), usually determined by combustion elemental analysis measurements and by X-ray photoelectron spectrometry. Unfortunately, in currently available graphene composite lithium ion battery cathode material characterizations little attention has been devoted to the characterization of graphene itself.

Raman spectra of graphene composite cathode materials usually have distinct carbon D and G bands located at 1350 and 1595 cm^{-1} respectively. Evaluating their intensities (I_D and I_G) can often help evaluating the ratio between graphene and other carbon species. As D band is a breathing mode of *k*-point phonons of A1g symmetry and G band is usually assigned to E2g phonon of C sp^2 hybridized atoms [145], the sp^3/sp^2 bond quantity in material can be estimated by measuring the ratio of D and G band intensities I_D/I_G. This helps to evaluate the amount of graphene relative to other carbon materials, as it is known that carbon atoms in graphene are sp^2 hybridized. Most of the studies suggest that lower I_D/I_G ratios provide higher cathode discharge capacity at high discharge rates [16,21,24,33,146]. Raman spectroscopy is even capable of determining the thickness of graphene nanosheets [147]. However, such evaluation is not possible for bulk cathode materials.

X-ray diffraction spectroscopy (XRD) is often used for lithium ion battery cathode material characterization. A peak corresponding to GO is located at 11° but is absent in most works after the reduction of GO. Usually no peaks associated with graphene are detected [17,18,22,31,32], although some report a peak at 26.5° corresponding to graphite [24] as a result of improper preparation of graphene nanosheets.

SEM and TEM are indispensable methods for visual material inspection, which can help in determining the dispersion of graphene nanosheets as well as their actual size and placement in the material. To better display the 3D graphene network, X. Zhou and colleagues have submersed their $LiFePO_4$/graphene sample in HCl, and thus $LiFePO_4$ has been etched so that only graphene remains [21]. It is then deduced with the help of TEM that the remaining graphene forms a 3D structure resembling a network, thus the assertions of several authors that the graphene nanosheets are known to make 3D electron conducting networks in the material [15–21,23–26,28,30,31] can be confirmed. The graphene network efficiently improves the electron transport in the material similarly to carbon nanotube (CNT) electron conducting networks reported earlier [14,148].

BET analysis results suggest that graphene increases surface areas of electrodes [22,28,30,32]. Although reduced graphene oxide surface area is far from the theoretical 2630 $m^2\ g^{-1}$ (684 $m^2\ g^{-1}$ [22], 420 $m^2\ g^{-1}$ [28]), significant increase in the electrode surface area is observed – 156 $m^2\ g^{-1}$ for $Li_3V_2(PO_4)_3$/C/rGO material measured versus 27 $m^2\ g^{-1}$ for $Li_3V_2(PO_4)_3$/C [30]; 16.8 for $m^2\ g^{-1}$ $Li_3V_2(PO_4)_3$/rGO versus 9.0 $m^2\ g^{-1}$ for $Li_3V_2(PO_4)_3$/C and 3.2 $m^2\ g^{-1}$ for $Li_3V_2(PO_4)_3$ with no additives [32].

A concise model of graphene composite cathode materials constructed after F.Y. Su et al. and C. Su et al. [15,25,35] is given in Fig. 2. Although graphene increases the electronic conductivity considerably, it can sometimes impede lithium ion migration and therefore impair charge capacity and rate capability [35] (see Fig. 2b). In a simulation made by F.Y. Su and colleagues it was determined that the path length that lithium ion travels from grain to grain increases when graphene is present in the material. Experimentally increased heating of the cell and decreased rate capability at high discharge rates were observed [35]. Regardless of this fact, most authors report increased rate capabilities for graphene-enhanced lithium ion battery cathode materials in their studies [15–24,26–34].

C. Su and colleagues reported that 2% graphene with no carbon black additives display poorer electrochemical performance than 2% graphene + 6% carbon black conducting additive, attributing the effect to only dotted contact of graphene sheets and active cathode material when no carbon black is present (see Fig. 2a and d) [15]. Zhou and colleagues observed similar effect in terms of electrochemical performance, when replacing half of the 5% graphene additive with glucose-derived carbon [21]. However, they attribute such electrochemical improvements to glucose-derived amorphous carbon species interrupting the stacking of graphene sheets [21].

Six structural models describing metal oxide/graphene composite material structure have been proposed by Z.S. Wu and colleagues (see Fig. 3). According to Z.S. Wu et al., the six structural models are:

(a) anchored model with nano-sized oxide particles anchored on graphene surfaces,

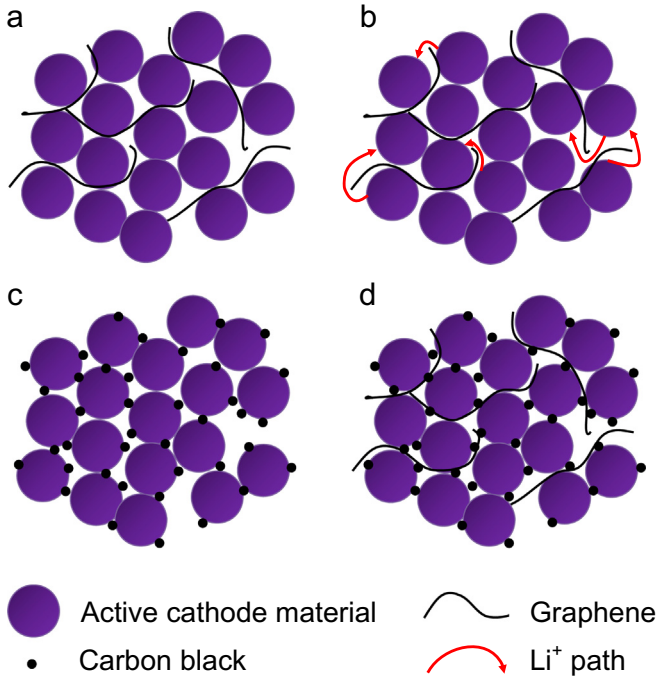

Fig. 2. A 2D model of (a) active cathode material with conductive graphene additive, (b) lithium pathways in active cathode material/graphene composite, (c) active cathode material/carbon black composite, (d) active cathode material/carbon black + graphene composite, drawn according to F.Y. Su et al. and C. Su et al. [15,25,35].

(b) wrapped model with metal oxide particles wrapped by graphene,
(c) encapsulated model with oxide particles encapsulated in graphene,
(d) sandwich-like model, where metal oxide particles are squeezed between two graphene layers creating a sandwich-like structure,
(e) layered model,
(f) mixed model where graphene and metal oxide particles mechanically mixed with graphene forming a conductive networking among the metal oxide particles [59].

After analyzing studies of lithium ion battery cathode material/graphene nanocomposites [15–34], we have found that such models can also be fitted for lithium ion battery cathode materials containing graphene (data summarized in Table 1). Most of the $LiFePO_4$/graphene composites produced possess a mixed structural model [15–18,20–25] with some containing graphene encapsulated [19,21] and anchored [20,22] $LiFePO_4$. Naturally, several $LiFePO_4$/graphene composites possess characteristics that can be assigned to several structural models [20–22]. Due to different means of material preparation as well as owing to the structural differences, $LiMn_2O_4$/graphene composites mostly appear to be anchored on graphene nanosheets [27–29]. In the studies of $Li_3V_2(PO_4)_3$/graphene composites it is assessed that mixed, anchored and wrapped structural models could apply [30–34]. However, it must be emphasized that in most of the studied graphene composite lithium ion battery cathodes, regardless of their structural model, authors conclude that a 3D electron conducting graphene networks have been formed, thus improving electron conductivity and electrochemical properties of the materials [15–21,23,24,26,28,30,31].

Although no specific research has been conducted on how to obtain a solely mixed or only anchored graphene composite cathode, it is known that the hydrophilic oxygen-containing functional groups (epoxides, hydroxides, carboxylic groups) on GO can serve as anchor sites and consequently make nanoparticles attach on the surfaces and edges of GO sheets [149]. Thus, when compared to pure graphene, GO and reduced GO are more likely to form an anchored structural model rather than mixed one. This is proven in an experiment with RuO_2 [150], where authors found that highly dispersed RuO_2 nanoparticles with a size less than 5 nm were formed on the surface of GO, while only large RuO_2 particles with a size ranging from tens to hundreds of nanometers were formed and sparsely distributed on the surface of CVD-grown graphene. There have been studies on $LiMPO_4$/functionalized CNT composites (M = Fe, Mn) [151,152], proving that multi-walled carbon nanotubes (MWCNTs) functionalized by carboxylic groups (MWCNTs-COOH), exhibit better affinity toward $LiMPO_4$. $LiFePO_4$/MWCNTs-COOH composite displayed improved charge capacity when compared to $LiFePO_4$/MWCNT cathode. $LiNi_{0.33}Co_{0.33}Mn_{0.33}O_2$ (NCM) composite displayed even more remarkable “anchoring effect” when combined with MWNCTs-COOH [152]. However,

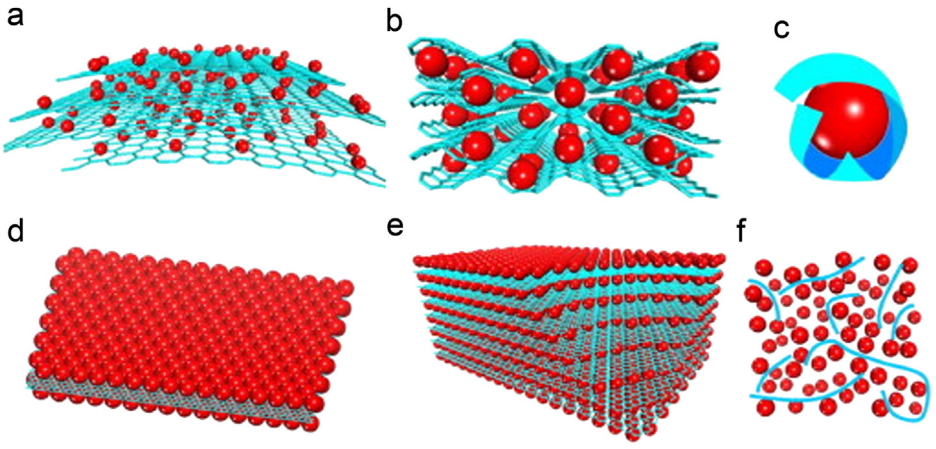

Fig. 3. Schematic of structural models of graphene/metal oxide composites: (a) Anchored model: nano-sized oxide particles anchored on graphene surfaces, (b) wrapped model: metal oxide particles wrapped by graphene, (c) encapsulated model: oxide particles encapsulated in graphene, (d) sandwich-like model: metal oxide particles are squeezed between two graphene layers creating a sandwich-like structure, (e) layered model: alternating layers of metal oxide nanoparticles and graphene, (f) mixed model: graphene and metal oxide particles mechanically mixed with graphene forming a conductive networking among the metal oxide particles. Red: metal oxide particles; blue: graphene sheets. Reprinted from Z.S. Wu et al. [56] with a permission from Elsevier. (For interpretation of the references to color in this figure legend, the reader is referred to the web version of this article.)

contrary to $LiFePO_4$, NCM/MWCNTs displayed better rate capability than NCM/MWNCTs-COOH. The authors claim that the electrochemical performance of NCM is affected by the formation of a passivation layer on the electrode surface, and that a reaction between NCM and MWCNTs-COOH could cause a coating of the active particles, which hinders the Li insertion/extraction [152]. According to these studies, conclusions can be drawn, that the structural model depends not only on the degree of graphene oxidation, but also on the active cathode material used.

4. Cathode electrochemical properties

4.1. $LiFePO_4$

Data available on $LiFePO_4$/graphene ($LiFePO_4$/G) composite cathode materials are summarized in Table 2. Rate capabilities of various $LiFePO_4$/G composites can be viewed in Fig. 4. As a qualitative indicator, specific discharge capacity improvement ratio has been shown in Fig. 4c. It has been calculated by dividing discharge capacities of graphene containing samples with discharge capacities of samples that do not contain any graphene. This has been done only for the studies where both graphene containing and graphene-free samples have been prepared.

$LiFePO_4$ samples tend to have a better rate capability when graphene is added to them. This is mainly due to the improvement in the electron conductivity. The increase of charge and discharge capacity is especially pronounced at large discharge rates (up to 50 C). Impedance spectra suggest that graphene reduces charge transfer resistance [15,17,18,20,25]. An interesting experiment was performed by Chang Su et al. [15] – 2 out of 8 wt.% of carbon additive were replaced by graphene. This changed the charge transfer resistance of the material from 300 Ω to 110 Ω thanks to better electron conductivity of the material.

Graphene makes unique 3D electron conducting networks within the material [15–21,23,24,26,28,30,31] which are somewhat like those made by CNTs [13,14,60,82,148,153]. Some studies also suggest that the rate capability is better when small amount of amorphous carbon is present in the material in addition to graphene [15,21]. Chang Su et al. [15] measured electrochemical properties of a material that contained 2% graphene nanosheets and no carbon coating. As this did not significantly improve the electrochemical characteristics of the material, authors concluded that graphene cannot form an effective conducting network within the $LiFePO_4$ due to only dotted contact between $LiFePO_4$ and graphene. This contact, according to their study, is improved when carbon coating is introduced [15]. However, after replacing half of the 5% graphene additive with glucose-derived carbon, X. Zhou et al. suggested that the improvement in discharge capacity is due to the glucose-derived carbon preventing the stacking of graphene sheets during synthesis [21]. It could also be true that some improvement was gained as smaller graphene content simply impedes lithium ion migration to a smaller extent [35]. In another research it was found that $LiFePO_4$ with 2% graphene additive provides better charge capacity than samples containing 1% or 4% and greater amount of graphene [25]. This could, of course, also be due to the stacking of graphene nanosheets.

$LiFePO_4$/G composites have a very high cyclability. Most of $LiFePO_4$/G materials show only a slight capacity fade (3% in 30 cycles at 0.1 C [15], 3% in 300 cycles at 5 C [19], 5% in 1000 cycles at 20 C (10 C charge current) [21]). This indicates that almost all $LiFePO_4$ remains electrochemically active during the cycling – presumably due to the improved electronic conductivity. No deeper

Table 2
Summary of the $LiFePO_4$/graphene composite material properties.

Additives		Additional additives for electrochemical measurements	Specific discharge capacity			Grain size	I_D/I_G in Raman spectra	Charge transfer resistance, Ω	Ref.
Graphene	Other carbon		0.1 C rate, mA h g^{-1}	10 C rate, mA h g^{-1}	10 C rate, per cents of 0.1 C				
2%	6%	20% carbon black, 10% PVDF	162	114 at 5 C[b]	–	200–400 nm	–	110	[15]
–	8%		141	52 at 5 C[b]	–	–		300	
2%	–		138	4 at 5 C[b]	–			850	
1%	6%	15% acetylene black, 10% PVDF	141	48	34%	100–180 nm	1.08	–	[16]
–	6%		103	35	34%	–	1.63		
13%	12%	12% carbon black, 8% PVDF	160	82	51%	30–250 nm	0.89	117	[17]
–	12%		160	55	34%	–	–	600	
5% graphene network[c]	–	5% acetylene black, 10% PVDF	158 at 0.2 C[a]	109	–	–	–	90	[18]
–			153 at 0.2 C[a]	42	–			170	
13% graphene encapsulation	–	10% acetylene black, 10% PVDF	167	91	54%	20 nm	–	–	[19]
8%	–	20% Super P, 10% PVDF	161	80	50%	150–400 nm	1.23	94	[20]
–			123	30	25%		–	175	
3%		10% Super P, 5% PVDF	143	65	45%			–	
8%			156	77	49%			–	
2.5%[c]	2.5%	15% Super P, 5% PVDF	150	122	81%	30–100 nm	1.14	–	[21]
5%[c]	–		147	129	88%		1.23		
–	5%		144	111	77%		1.00		
1.5%	–	10% carbon black, 10% PVDF	160 at 0.2 C[a]	109	–	20 nm	–	–	[22]
5%	–	10% acetylene black, 10% PTFE	161	116	72%	200 nm	–	–	[23]
–			128	62	48%	–			
1.4%	22.8%	10% carbon black, 10% PVDF	159	–	–	–	1.04	–	[24]
–			152				1.13		
0.5%	–	PTFE (precise amount not given)	137	–	–	–	–	–	[25]
2%			151					148	
6%			138					162	
20%			133					249	
–	20%		142					169	

[a] Result given for 0.2 C discharge rate, as no 0.1 C measurement data are available.
[b] Result given for 5 C discharge rate, as no 10 C measurement data are available.
[c] Graphene added after $LiFePO_4$ synthesis.

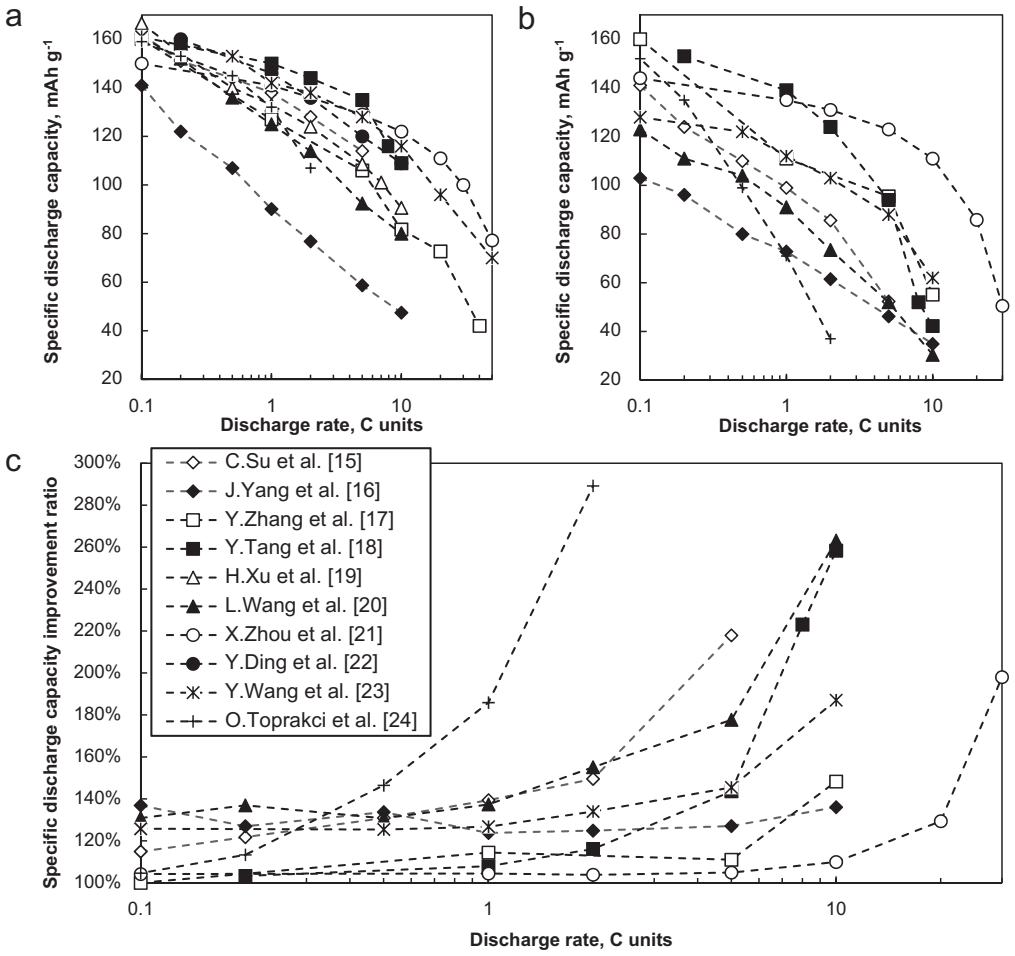

Fig. 4. Specific discharge capacities of (a) $LiFePO_4$/graphene composite materials, (b) reference samples prepared by the respective authors. (c) Specific discharge capacity improvement for $LiFePO_4$/graphene composites vs. reference samples [15–24].

analysis has been carried out for any of the $LiFePO_4$/G composites to clarify the exact cause of the superior cyclability, but it is known that improved electronic contact between the particles can indeed improve cyclability [154–156]. However, it is worth noting that nanocrystalline $LiFePO_4$ with no carbon additives (grain width and length approximately 20 and 50 nm respectively) can also display excellent cyclability [157]. In addition, the capacity fade of $LiFePO_4$ can sometimes be so negligible that, in conventional batteries, the electrochemical performance would primarily decline because of structural changes in the anode rather than in the cathode [158].

For most experiments samples are being prepared by mixing the active material with additional 5–20% of carbon and 5–10% of PVDF. Some of the works have raised the question of whether such variations in sample preparation can influence the electrochemical characteristics obtained [20,25,35]. By varying the carbon content added for electrochemical measurements, L. Wang et al. have shown that at least in their case the effects are almost negligible [20] (see Table 2). However, a different $LiFePO_4$ study suggests that the doubling of carbon content added during electrode preparation (carbon content increased from 10 to 20 wt.%) could have considerable impact on the charge capacity as well as rate capability measured [159]. This is also the main reason why the electrode preparation is included as a separate column in Table 2.

Differences between $LiFePO_4$/G material discharge capacities vary from 133 mA h g^{-1} [16] to 167 mA h g^{-1} [15] at 0.1 C rate. Differences over reference samples are considerable – graphene containing $LiFePO_4$ materials possess 110% [21] to 260% [18,20] of the discharge capacity of graphene non-containing samples at 10 C rate. Naturally, some question arising are – what are the main factors affecting the electrochemical performance and how can $LiFePO_4$/G composite material with the best electrochemical performance be prepared?

Rate capability and charge capacity of a material can be improved in several ways, most considerable of which are decreasing the grain size, thus shortening the lithium ion migration path and increasing electrode surface area [6,10,157,160,161], improving electronic conductivity by addition of electrochemical additives [8,12,79] and to some extent also doping [8,80,162–164]. The effect of smaller grain size appears to be true when looking at the results in Table 2. Nevertheless, it is also clear that there are other factors influencing the charge capacity and rate capability of the $LiFePO_4$/G composites, such as the mixing technique of electron conducting additives [165] as well as the size, conductivity and distribution of graphene nanosheets [58,111]. Unfortunately, most of them cannot or simply are not expressed quantitatively in most published works.

Regarding the mixing of graphene into the active cathode material, there is no evidence to say that either one structural model (see Fig. 3) provides larger charge capacity or rate capability than others. Apparently there are too many factors influencing electrochemical properties of $LiFePO_4$. Also, no single best synthesis method can be deduced for $LiFePO_4$/G preparation, and there is not enough statistical data to do so. Still, the solid state route seems to yield the most consistent and best results regarding the rate

capability (see Refs. [18,23]). Experimental works tend to suggest that if tight particle encapsulation is not required, mixing of active cathode material and GO can be done after the active cathode material synthesis [18,21]. Nevertheless, proper mixing and GO reduction are still prerequisites for superior electrochemical performance.

As it can be seen in Fig. 4a, X. Zhou et al. [21] have obtained the $LiFePO_4$/C/G nanocomposite with one of the best rate capabilities. However, it must be emphasized that charge and discharge rates in their experiment were identical only until 10 C. After that the charge current was kept at 10 C independent from the discharge rate. The authors account the superior rate capability of their $LiFePO_4$/C/G material to three factors – firstly, small grain size (shorter diffusion path reduces the time needed for Li^+ to migrate between the cathode and electrolyte and increase the surface area), secondly, graphene with higher degree of graphitization being more advantageous in increasing the electron conductivity than the conventional carbon coating and, thirdly, 3D graphene conducting network wrapping the $LiFePO_4$ particles [21]. In their work 3 different $LiFePO_4$ samples were prepared with 5 wt.% graphene nanosheets and no carbon coating, 2.5 wt.% graphene nanosheets and 2.5 wt.% carbon coating and with 5 wt.% carbon coating and no graphene at all. The sample containing 2.5 wt.% graphene nanosheets and 2.5 wt.% carbon coating showed the best discharge capacity and superb rate capability (47% of the 0.1 C capacity still available at 60 C discharge current). The improved electrochemical properties of $LiFePO_4$/G/C material is said to be thanks to the glucose-derived amorphous carbon interrupting the stacking of graphene sheets [21]. It is partially in agreement with F.Y. Su et al., who conclude that too large graphene concentration can indeed hinder the migration of lithium ions in the cathode [35].

A more non-standard route has been chosen by H. Xu and colleagues and Y. Tang et al. [18,19]. H. Xu and colleagues obtain graphene encapsulated $LiFePO_4$ by first encapsulating FeOOH particles with GO and then carrying on with a solid state synthesis [19]. Y. Tang et al. have used chemical vapor deposition to deposit 3D, highly crystalline graphene-like structures on a porous Ni template [18]. After Ni is removed, these graphene structures are mixed with $LiFePO_4$. This composite cathode has improved discharge capacity and rate capability when compared to the reference material prepared by the authors.

Of course, there are other ways of improving rate capability of $LiFePO_4$. Some of them include carbon coating of particles [79], adding polypyrrole (PPy) [81], adding MWCNTs [82,153], doping $LiFePO_4$ [80,162] and creating various micro- and nanostructures [83,166]. Best results obtained by these methods have been compared with $LiFePO_4$/G composites (see Fig. 5).

Ni doped and carbon coated cathode obtained by Y. Ge et al. [80] seems to have better rate performance at up to 15 C than offered by $LiFePO_4$/G nanocomposites. Carbon coated $LiFePO_4$ obtained by M. Konarova et al. [79] outperform $LiFePO_4$/G only at discharge rates higher than 40 C. Most studies, however, obtain materials with worse rate capabilities than those of at least some $LiFePO_4$/G materials [81–83]. It must be taken into account, that reference $LiFePO_4$ samples discussed here are among the best of their kind and synthesis routes required to produce such samples can often be very complex. Thus graphene addition is one of the best methods and most certainly one of the most efficient electrically conductive additives that can be used in order to increase the discharge capacity of $LiFePO_4$ when discharging at high discharge rates.

4.2. Other $LiMPO_4$ type materials

Although $LiFePO_4$/G is certainly the most researched $LiMPO_4$/G type material (M – transition metal), considerable effort has been devoted to other phosphate cathode materials [26,30–34], mostly $Li_3V_2(PO_4)_3$/G ($Li_3V_2(PO_4)_3$/graphene) composites [30–34]. The summary of available studies on $LiMPO_4$/G composites can be seen in Table 3 and Fig. 6. It is necessary to note that $Li_3V_2(PO_4)_3$ is often discharged in two voltage ranges – 3.0–4.3 V and 3.0–4.8 V. During the charging process in voltage range of 3.0–4.3 V two lithium ions can be reversibly extracted from $Li_3V_2(PO_4)_3$ based on the V^{3+}/V^{4+} redox couple, yielding a theoretical charge capacity of 133 mA h g^{-1}. Third lithium ion can be extracted at approximately 4.52 V, making $Li_3V_2(PO_4)_3$ the phosphate material with the largest theoretical capacity – 197 mA h g^{-1}, in such case, however, the voltage range needs to be increased to 3.0–4.8 V. The extraction of the third lithium ion is kinetically difficult, as the ionic and electronic conductivities of completely delithiated phase, $V_2(PO_4)_3$, are much lower [167]. It must also be noted that several difficulties can arise, such as electrolyte oxidation, a significant overpotential during this voltage window [31] and vanadium dissolution into the electrolyte at deep oxidation potential of 4.6 V vs. Li [168,169].

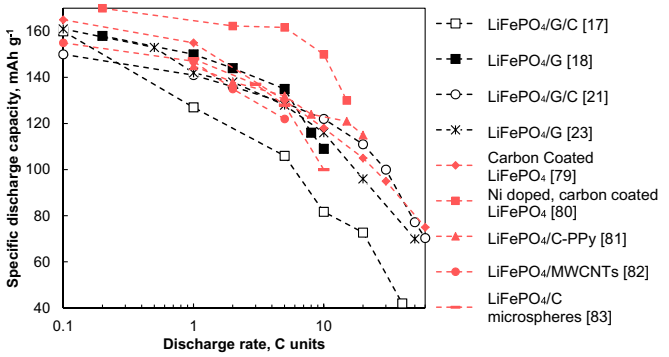

Fig. 5. Specific discharge capacities of the best of the $LiFePO_4$/graphene composites and other $LiFePO_4$ materials with high rate capabilities [17,18,21,23,79–83].

Similarly to $LiFePO_4$, all other $LiMPO_4$/G composites perform better when compared to their reference samples [26,30–32,34]. This is most pronounced at large discharge rates and serves as a proof that graphene can improve the rate capability of cathode materials. Similarly to $LiFePO_4$, the combination of both graphene and carbon seems to provide the best results for $Li_3V_2(PO_4)_3$, suggesting that the less crystalline carbon species interrupt the stacking of graphene layers [31]. It is also found that carbon coating is still necessary, as it not only acts as a conductive additive improving the electronic conductivity of $Li_3V_2(PO_4)_3$, but also forms a barrier to prevent the direct contact between $Li_3V_2(PO_4)_3$ particles and the electrolyte, hence minimizing the vanadium dissolution into the electrolyte [31,169]. The EIS results suggest that graphene decreases charge transfer resistance more effectively than conventional carbon additives [32].

Cycling stability is also improved for $Li_3V_2(PO_4)_3$/G composites [30,31,33,34]. Virtually no capacity loss during first 100 cycles is observed for $Li_3V_2(PO_4)_3$/G/C composites at charge and discharge rate of 0.5 C when charging until 4.3 V, and a remarkable 91% capacity retention at 0.2 C charge/discharge rate is observed in the 100th cycle in a voltage range of 3.0–4.8 V for $Li_3V_2(PO_4)_3$/G/C composite [30]. Y. Jiang and colleagues observe 98% capacity retention after 100 cycles at 0.1 C rate for $Li_3V_2(PO_4)_3$/C/G material in a voltage range of 3.0–4.3 V (only 83% capacity retention was observed for $Li_3V_2(PO_4)_3$/C) [31]). Similarly good cycling performance was observed by J. Zhu et al. – 88% capacity retention at 0.5 C rate in 50th cycle, voltage range – 3.0–4.8 V [33]. H. Liu et al. reported virtually no capacity loss during first 100 cycles at 0.1, 1 and 2 C discharge rates in voltage range of 3.0–4.3 V and approximately 80% capacity retention for the aforementioned discharge rates when charged and discharged until 4.8 and 3.0 V respectively.

Table 3
Summary of the $LiMPO_4$/graphene composite material properties.

Material	Additives		Additional additives for electrochemical measurements	Specific discharge capacity, mA h g^{-1}		Grain size	Ref.
	Graphene	Other carbon		Lowest discharge rate	Highest discharge rate		
$LiMn_{0.75}Fe_{0.25}PO_4$ nanorods on graphene nanosheets	20%	6%	None	155 at 0.5 C	65 at 100 C	Nanorods with 50–100 nm length, 20–30 nm width	[26]
$Li_3V_2(PO_4)_3$	12%	17%	None	127/168 at 1 C[a]	90 at 50 C/109 at 30 C[a]	5–8 nm	[30]
	–	17%	10% carbon black, 10% PVDF	123 at 1 C[b]	15 at 40 C[b]	100–500 nm	
$Li_3V_2(PO_4)_3$	15%	–	10% acetylene black, 5% PTFE	125/174 at 0.1 C[a]	104/108 at 5 C[a]	100–200 nm	[31]
	Total amount – 15%			131/182 at 0.1 C[a]	109/118 at 5 C[a]	50–150 nm	
	–	15%		111/133 at 0.1 C[a]	80/52 at 5 C[a]	–	
$Li_3V_2(PO_4)_3$	1.1%	–	30% super P, 10% PVDF	129 at 0.1 C[b]	46 at 50 C[b]	10–40 nm	[32]
	–	2.7%		109 at 0.1 C[b]	48 at 20 C[b]	–	
	–	–		114 at 0.1 C[b]	50 at 5 C[b]	30–100 nm	
$Li_3V_2(PO_4)_3$	3%	–	10% carbon black, 10% PVDF	177 at 0.5 C[c]	137 at 5 C[c]	500–1000 nm	[33]
$Li_3V_2(PO_4)_3$	1.1%	–	30% super P, 10% PVDF	128/168 at 0.1 C[b]	82 at 50 C/150 at 2 C[b]	280 nm	[34]
	–	–		120/123 at 0.1 C[b]	90 at 5 C/40 at 2 C[a]	669 nm	

[a] First result for charge/discharge voltages 3.0–4.3 V, second for 3.0–4.8 V.
[b] Result given for voltage range 3.0–4.3 V.
[c] Result given for voltage range 3.0–4.8 V.

In studies regarding $Li_3V_2(PO_4)_3$/G composites GO or partially reduced GO is mixed with a precursor, thus mostly obtaining structures, where active cathode material particles are anchored on graphene nanosheets. It appears that the factor influencing the electrochemical properties the most, is the grain size, smaller grain sizes consequentially yielding better rate capabilities [30–33], with 5–8 nm nanoparticles providing the best rate capability [30]. The authors have also created a structure where $Li_3V_2(PO_4)_3$ is embedded in a nanoporous carbon matrix, which is attached to graphene sheets [30].

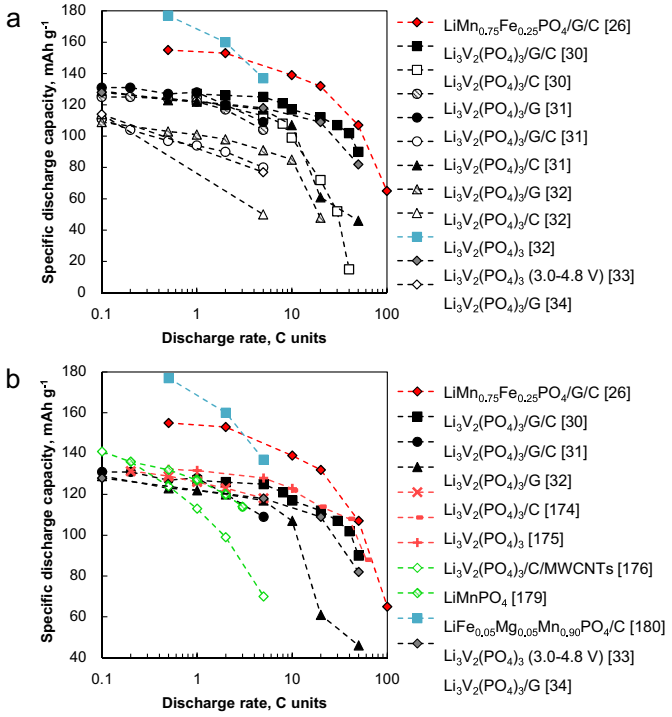

Fig. 6. Specific discharge capacities of (a) $LiMPO_4$/graphene composite materials and their reference samples if available [26,30–34], (b) $LiMPO_4$/graphene composite materials and other $LiMPO_4$ materials [26,30–34,174–176,179,180]; $Li_3V_2(PO_4)_3$ discharged in voltage range 3.0–4.3 V if not indicated otherwise.

When compared to most other $Li_3V_2(PO_4)_3$ studies where various methods for improving discharge capacity and rate performance have been used [170–173], graphene appears to be one of the best methods for improving such electrochemical properties. However, it is worth noting that some other methods offer similar or improved discharge capacity even at high discharge rates. H. Wang et al. have prepared $Li_3V_2(PO_4)_3$/C (C content – 2 wt.%) with a polyvinylpyrrolidone-assisted sol–gel method [174], L. Zhang et al. have prepared nanoporous $Li_3V_2(PO_4)_3$/C (C content – 5.4 wt.%) via sol–gel-combustion method [175], $Li_3V_2(PO_4)_3$/C/MWCNTs composite can also reach remarkable discharge capacities at high discharge currents [176] (see details in Fig. 6). These results also offer excellent rate capability, thus challenging the use of graphene additives as a method for improving electrochemical characteristics of the cathode.

$LiMnPO_4$/G composites have also been studied as a cathode for rechargeable lithium ion batteries. H. Wang et al. have prepared $LiMn_{1-x}Fe_xPO_4$ nanorods (length of 50–100 nm and width of 20–30 nm) on reduced graphene oxide sheets (oxide content lower than usually acquired by Hummers method [26]), determining that the $LiMn_{0.75}Fe_{0.25}PO_4$ ($x = 0.25$) provides excellent discharge capacity at discharge currents as high as 100 C (see Fig. 6a and b). Their results suggested that mildly oxidized graphene sheets presented a unique substrate for growing nanocrystals into well-defined morphologies, such as nanoplates and nanorods [26]. The unique combination of nano-sized particles, doping and improved GO preparation and reduction method have yielded superior rate capability that is hard to obtain with other methods [177–180], as even at 100 C discharge rate remarkable 65 mA h g^{-1} discharge capacity can be achieved.

4.3. $LiMn_2O_4$

$LiMn_2O_4$ is a spinel type cathode material. Proposed for use in lithium ion batteries in 1983 [181], it is now being used in several commercial electrical vehicle batteries [182] due to its low production cost, environmental friendliness and good safety characteristics [182,183]. A pronounced problem for $LiMn_2O_4$, however, is its relatively low cyclability. Mn^{2+} dissolution in the electrolyte and formation of a new, less symmetrical and more disordered phase during the first Li deinsertion are obstacles that contribute to the loss of cyclability of the material [184–186]. Various coatings

Table 4
Summary of the $LiMn_2O_4$/graphene composite material properties.

Additives		Additional additives for electrochemical measurements	Specific discharge capacity, mA h g^{-1}		Grain size	Ref.
Graphene	Other carbon		Lowest discharge rate	Highest discharge rate		
27%	–	10% acetylene black, 5% PVDF	137 at 1 C	101 at 100 C	10–40 nm	[28]
45%	–	10% PVDF	108 at 1.27 C	51.5 at 127 C	3–10 nm	[29]

appear to partially hinder the Mn^{2+} dissolution [90,187,188]. Studies of $LiMn_2O_4$/G ($LiMn_2O_4$/graphene) composite materials are summarized in Table 4 and Fig. 7.

S.-M. Bak et al. have prepared a nanocrystalline $LiMn_2O_4$/G (27 wt.%) cathode material with remarkable discharge capacity high rate capability, 90% discharge capacity retention at 1 C rate over 100 cycles and 96% discharge capacity retention at 10 C over 100 cycles. Excellent electrochemical properties are claimed to be connected with a good dispersion of the reduced graphene oxide nanosheet template and reduced graphene oxide sheets serving as a 3D electron conducting network [28]. Additionally, high $LiMn_2O_4$ particle active surface area has been maintained and the $LiMn_2O_4$ particles are nano-sized [28].

W. Zhang et al. have produced $LiMn_2O_4$/G nanocomposites with grain sizes as small as 3.2 nm and graphene nanosheet content as high as 45% [29]. Their rate capability, however, is poorer than that of $LiMn_2O_4$/G composite obtained by J.G. Kim et al. [27]. Nevertheless, it is superior when authors compare it to a commercially available $LiMn_2O_4$ [29] and also superior to nanocrystalline $LiMn_2O_4$ [189] (one of the best results regarding rate capability). In contrast to the results obtained by F.Y. Su et al. for $LiFePO_4$, where graphene in large concentrations was found to reduce cathode material ($LiFePO_4$/G) discharge capacity [25], study by W. Zhang et al. suggests decreased charge transfer resistance and higher discharge capacities for materials with higher graphene content [29]. This could be connected with the quality of their graphene preparation methods (electrochemical graphene exfoliation [29] vs. vacuum-promoted low-temperature approach [25]), different graphene dispersion in the cathode (anchored [29] vs. mixed [25] structure, see Table 1) or simply different lithium ion intercalation kinetics, as the active cathode material is $LiMn_2O_4$, not $LiFePO_4$. Discharge capacity is found not to be reduced during first 100 cycles at 1.27 C, 6.33 and 38.01 C discharge rates. It is found that graphene additive reduces Mn^{2+} dissolution into the electrolyte [29].

When compared with other studies where no graphene electron conducting additives are used (see Fig. 7), it is difficult to find results better than those obtained by W. Zhang et al. for $LiMn_2O_4$/G nanocomposite [28]. However, some of the most remarkable results regarding $LiMn_2O_4$ with superior rate capability have been obtained by Y. Chen and colleagues, who have studied nanocrystalline $LiMn_2O_4$ with grain size of about 60 nm [189]. H. Xia et al. have prepared $LiMn_2O_4$/MWCNT nanocomposites (10–20 nm particles, about 20% CNT content) [190], W. Tang et al. obtained $LiMn_2O_4$ nanochains, composed of 100 nm particles [191].

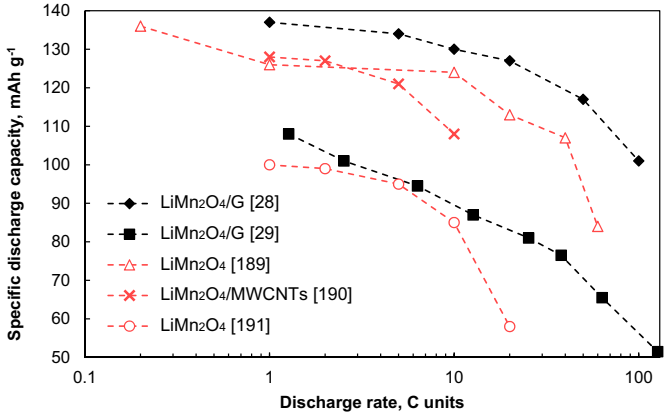

Fig. 7. Specific discharge capacities of high rate capability $LiMn_2O_4$ cathode materials [28,29,189–191].

5. Conclusions

Graphene forms a 3D electron conducting network in lithium ion battery cathode materials when mixed properly. This increases electron conductivity and therefore rate capability and cyclability of the materials. However, when mixed improperly or used in excessive amounts, it can sometimes impede lithium ion migration. Nevertheless, graphene could be one of the best materials used as conductive additives for lithium ion battery cathode materials. Given the superiority of graphene over the conventional carbon electron conducting additives, one would expect its widespread use in commercially available high power lithium ion batteries. However, it must also be noted that the rather complicated synthesis and therefore the high price of GO nanosheets could limit its use in commercial applications.

The characterization of graphene used in studies researching it as an electron conducting additive for lithium ion battery cathode materials is often deficient. The importance of proper graphene preparation and characterization cannot be overlooked. The preparation of graphene with large electron conductivity is of paramount importance. As in most cases GO is used, appropriate reduction of GO must be carried out. By varying material preparation parameters, several graphene composite structures can be obtained, such as active cathode material particles anchored on graphene, mixed with graphene, wrapped or encapsulated in graphene. It is still unclear, which of these structures offer better cathode electrochemical properties. Small addition of conventional carbon additives appears to hinder the stacking of graphene layers, thus improving cathode electrochemical performance.

Although graphene appears to be one of the best electron conducting additives due to its high electron conductivity and large specific surface area, several additional methods can be used in order to improve lithium ion battery cathode charge capacity and rate capability – most considerably grain size reduction, addition of electron or lithium ion conducting additives and sometimes doping. They allow obtaining similar high power lithium ion battery cathode materials with improved rate capability and excellent cyclability. However, the preparation of such materials can be rather complex, even when compared with graphene composite cathode materials. A combination of graphene nanosheets as electron conducting additive, nano-sized active cathode material particles, conventional less crystalline carbon additives and doping appears to provide electrochemical properties difficult to achieve otherwise at least in one case (Ref. [26]), thus suggesting a possible way of further improving lithium ion battery cathode material rate performance and cyclability.

Acknowledgments

Authors acknowledge Taiwan–Latvia–Lithuania cooperation project "Materials and processing development for advanced Li ion batteries" for financial support. G. Kucinskis acknowledges National program in material sciences.

References

[1] Y. Nishi, J. Power Sources 100 (2001) 101.
[2] K. Mizushima, P.C. Jones, P.J. Wiseman, J.B. Goodenough, Solid State Ionics 3–4 (1981) 171.
[3] M.G.S.R. Thomas, P.G. Bruce, J.B. Goodenough, Solid State Ionics 17 (1985) 13.
[4] B. Scrosati, J. Garche, J. Power Sources 195 (2010) 2419.
[5] S.J. Dillon, K. Sun, Curr. Opin. Solid State Mater. Sci. 16 (2012) 153.
[6] M. Park, X. Zhang, M. Chung, G.B. Less, A.M. Sastry, J. Power Sources 195 (2010) 7904.
[7] Z. Ma, G. Shao, G. Wang, J. Du, Y. Zhang, Ionics 19 (2013) 437.
[8] H. Zhang, Y. Xu, C. Zhao, X. Yang, Q. Jiang, Electrochim. Acta 83 (2012) 341.
[9] B. Pei, H. Yao, W. Zhang, Z. Yang, J. Power Sources 220 (2012) 317.
[10] F.F.C. Bazito, R.M. Torresi, J. Braz. Chem. Soc. 17 (2006) 627.
[11] Q. Cao, H.P. Zhang, G.J. Wang, Q. Xia, Y.P. Wu, H.Q. Wu, Electrochem. Commun. 9 (2007) 1228.
[12] A. Fedorková, R. Oriňáková, A. Oriňák, M. Kupková, H.-D. Wiemhöfer, J.N. Audinot, J. Guillot, Solid State Sci. 14 (2012) 1238.
[13] X. Sun, J. Li, C. Shi, Z. Wang, E. Liu, C. He, X. Du, N. Zhao, J. Power Sources 220 (2012) 264.
[14] X.-M. Liu, Z.-D. Huang, S.-W. Oh, B. Zhang, P.-C. Ma, M.M.F. Yuen, J.-K. Kim, Compos. Sci. Technol. 72 (2012) 121.
[15] C. Su, X. Bu, L. Xu, J. Liu, C. Zhang, Electrochim. Acta 64 (2012) 190.
[16] J. Yang, J. Wang, D. Wang, X. Li, D. Geng, G. Liang, M. Gauthier, R. Li, X. Sun, J. Power Sources 208 (2012) 340.
[17] Y. Zhang, W. Wang, P. Li, Y. Fu, X. Ma, J. Power Sources 210 (2012) 47.
[18] Y. Tang, F. Huang, H. Bi, Z. Liu, D. Wan, J. Power Sources 203 (2012) 130.
[19] H. Xu, J. Chang, J. Sun, L. Gao, Mater. Lett. 83 (2012) 27.
[20] L. Wang, H. Wang, Z. Liu, C. Xiao, S. Dong, P. Han, Z. Zhang, X. Zhang, C. Bi, G. Cui, Solid State Ionics 181 (2010) 1685.
[21] X. Zhou, F. Wang, Y. Zhu, Z. Liu, J. Mater. Chem. 21 (2011) 3353.
[22] Y. Ding, Y. Jiang, F. Xu, J. Yin, H. Ren, Q. Zhuo, Z. Long, P. Zhang, Electrochem. Commun. 12 (2010) 10.
[23] Y. Wang, Z.-S. Feng, J.-J. Chen, C. Zhang, Mater. Lett. 71 (2012) 54.
[24] O. Toprakci, H.A.K. Toprakci, L. Ji, Z. Lin, R. Gu, X. Zhang, J. Renew. Sustain. Energy 4 (2012) 013121.
[25] F.-Y. Su, C. You, Y.-B. He, W. Lv, W. Cui, F. Jin, B. Li, Q.-H. Yang, F. Kang, J. Mater. Chem. 20 (2010) 9644.
[26] H. Wang, Y. Yang, Y. Liang, L.-F. Cui, H.S. Casalongue, Y. Li, G. Hong, Y. Cui, H. Dai, Angew. Chem. Int. Ed. 50 (2011) 7364.
[27] J.-G. Kim, H.-K. Kim, J.-P. Jegal, K.-H. Kim, J.-Y. Kim, S.-H. Park, K.-B. Kim, in: Proceedings of the International Conference Nanomaterials: Applications and Properties, vol. 1, 2012, p. 04NEA07.
[28] S.-M. Bak, K.-W. Nam, C.-W. Lee, K.-H. Kim, H.-C. Jung, X.-Q. Yang, K.-B. Kim, J. Mater. Chem. 21 (2011) 17309.
[29] W. Zhang, Y. Zeng, C. Xu, N. Xiao, Y. Gao, L.-J. Li, X. Chen, H.H. Hng, Q. Yan, Beilstein J. Nanotechnol. 3 (2012) 513.
[30] X. Rui, D. Sim, K. Wong, J. Zhu, W. Liu, C. Xu, H. Tan, N. Xiao, H.H. Hng, T.M. Lim, Q. Yan, J. Power Sources 214 (2012) 171.
[31] Y. Jiang, W. Xu, D. Chen, Z. Jiao, H. Zhang, Q. Ma, X. Cai, B. Zhao, Y. Chu, Electrochim. Acta 85 (2012) 377.
[32] H. Liu, G. Yang, X. Zhang, P. Gao, L. Wang, J. Fang, J. Pinto, X. Jiang, J. Mater. Chem. 22 (2012) 11039.
[33] J. Zhu, R. Yang, K. Wu, Ionics (2012), http://dx.doi.org/10.1007/s11581-012-0795-8.
[34] H. Liu, P. Gao, J. Fang, G. Yang, Chem. Commun. 47 (2011) 9110.
[35] F.-Y. Su, Y.-B. He, B. Li, X.-C. Chen, C.-H. You, W. Wei, W. Lv, Q.-H. Yang, F. Kang, Nano Energy 1 (2012) 429.
[36] D.R. Cooper, B. D'Anjou, N. Ghattamaneni, B. Harack, M. Hilke, A. Horth, N. Majlis, M. Massicotte, L. Vandsburger, E. Whiteway, V. Yu, ISRN Condens. Matter Phys. 2012 (2012) 501686.
[37] K.S. Novoselov, A.K. Geim, S.V. Morozov, D. Jiang, Y. Zhang, S.V. Dubonos, I.V. Grigorieva, A.A. Firsov, Science 306 (2004) 666.
[38] A.T.S. Wee, ACS Nano 6 (2012) 5739.
[39] L. Grande, V.T. Chundi, D. Wei, C. Bower, P. Andrew, T. Ryhänen, Particuology 10 (2012) 1.
[40] K.I. Bolotin, K.J. Sikes, Z. Jiang, M. Klima, G. Fudenberg, J. Hone, P. Kim, H.L. Stormer, Solid State Commun. 146 (2008) 351.
[41] M.D. Stoller, S. Park, Y. Zhu, J. An, R.S. Ruoff, Nano Lett. 8 (2008) 3498.
[42] M. Zhou, Y. Zhai, S. Dong, Anal. Chem. 81 (2009) 5603.
[43] L. Valentini, M. Cardinali, S. Bittolo Bon, D. Bagnis, R. Verdejo, M.A. Lopez-Manchado, J.M. Kenny, J. Mater. Chem. 20 (2010) 995.
[44] B. Tang, G. Hu, J. Power Sources 220 (2012) 95.
[45] Y.-J. Jeon, J.-M. Yun, D.-Y. Kim, S.-I. Na, S.-S. Kim, Sol. Energy Mater. Sol. Cells 105 (2012) 96.
[46] L. Qu, Y. Liu, J.-B. Baek, L. Dai, ACS Nano 4 (2010) 1321.
[47] B. Seger, P.V. Kamat, J. Phys. Chem. C 113 (2009) 7990.
[48] M.S. Ahmed, S. Jeon, J. Power Sources 218 (2012) 168.
[49] J. Yan, T. Wei, B. Shao, Z. Fan, W. Qian, M. Zhang, F. Wei, Carbon 48 (2010) 487.
[50] J.J. Yoo, K. Balakrishnan, J. Huang, V. Meunier, B.G. Sumpter, A. Srivastava, M. Conway, A.L.M. Reddy, J. Yu, R. Vajtai, P.M. Ajayan, Nano Lett. 11 (2011) 1423.
[51] B. Jiang, C. Tian, L. Wang, L. Sun, C. Chen, X. Nong, Y. Qiao, H. Fu, Appl. Surf. Sci. 258 (2012) 3438.
[52] E. Yoo, H. Zhou, ACS Nano 5 (2011) 3020.
[53] Y. Li, J. Wang, X. Li, D. Geng, R. Li, X. Sun, Chem. Commun. 47 (2011) 9438.
[54] J. Xiao, D. Mei, X. Li, W. Xu, D. Wang, G.L. Graff, W.D. Bennett, Z. Nie, L.V. Saraf, I.A. Aksay, J. Liu, J.-G. Zhang, Nano Lett. 11 (2011) 5071.
[55] S.-M. Paek, E. Yoo, I. Honma, Nano Lett. 9 (2009) 72.
[56] P. Lian, X. Zhu, S. Liang, Z. Li, W. Yang, H. Wang, Electrochim. Acta 55 (2010) 3909.
[57] M. Sathish, T. Tomai, I. Honma, J. Power Sources 217 (2012) 85.
[58] D.A.C. Brownson, D.K. Kampouris, C.E. Banks, J. Power Sources 196 (2011) 4873.
[59] Z.-S. Wu, G. Zhou, L.-C. Yin, W. Ren, F. Li, H.-M. Cheng, Nano Energy 1 (2012) 107.
[60] S.L. Candelaria, Y. Shao, W. Zhou, X. Li, J. Xiao, J.-G. Zhang, Y. Wang, J. Liu, J. Li, G. Cao, Nano Energy 1 (2012) 195.
[61] C. Liu, A. Zhamu, D. Neff, B.Z. Jang, Lithium Super-Battery with a Functionalized Nano Graphene Cathode, U.S. Patent US20120045688, 2010.
[62] D. Choi, J. Liu, Z. Yang, W. Wang, G.L. Graff, Graphene/$LiFePO_4$ Cathode with Enhanced Stability, U.S. Patent US20120164534, 2010.
[63] A. Zhamu, J. Shi, G. Chen, M.C. Wang, B.Z. Jang, Graphene-Enhanced Cathode Materials for Lithium Batteries, U.S. Patent US20120058397, 2010.
[64] K. Dokko, M. Mohamedi, Y. Fujita, T. Itoh, M. Nishizawa, M. Umeda, I. Uchida, J. Electrochem. Soc. 148 (2001) A422.
[65] J. Barker, R. Pynenburg, R. Koksbang, M.Y. Saidi, Electrochim. Acta 41 (1996) 2481.
[66] S. Levasseur, M. Ménétrier, C. Delmas, Chem. Mater. 14 (2002) 3584.
[67] J. Marzec, K. Świerczek, J. Przewoźnik, J. Molenda, D.R. Simon, E.M. Kelder, J. Schoonman, Solid State Ionics 146 (2002) 225.
[68] F. Cao, J. Prakash, Electrochim. Acta 47 (2002) 1607.
[69] P.P. Prosini, M. Lisi, D. Zane, M. Pasquali, Solid State Ionics 148 (2002) 45.
[70] S. Shi, L. Liu, C. Ouyang, D.-S. Wang, Z. Wang, L. Chen, X. Huang, Phys. Rev. B 68 (2003) 195108.
[71] A. Pan, D. Choi, J.-G. Zhang, S. Liang, G. Cao, Z. Nie, B.W. Arey, J. Liu, J. Power Sources 196 (2011) 3646.
[72] A.K. Padhi, K.S. Nanjundaswamy, J.B. Goodenough, J. Electrochem. Soc. 144 (1997) 1188.
[73] B. Lin, Z. Wen, Z. Gu, S. Huang, J. Power Sources 175 (2008) 564.
[74] J.W. Fergus, J. Power Sources 195 (2010) 939.
[75] Y. Zhang, C.-Y. Wang, X. Tang, J. Power Sources 196 (2011) 1513.
[76] G. Bajars, G. Kucinskis, J. Smits, J. Kleperis, Solid State Ionics 188 (2011) 156.
[77] J. Smits, G. Kucinskis, G. Bajars, J. Kleperis, Latvian J. Phys. Tech. Sci. 48 (2011) 27.
[78] F. Sauvage, E. Baudrin, M. Morcrette, J.-M. Tarascon, Electrochem. Solid-State Lett. 7 (2004) A15.
[79] M. Konarova, I. Taniguchi, J. Power Sources 195 (2010) 3661.
[80] Y. Ge, X. Yan, J. Liu, X. Zhang, J. Wang, X. He, R. Wang, H. Xie, Electrochim. Acta 55 (2010) 5886.
[81] Y. Yang, X.-Z. Liao, Z.-F. Ma, B.-F. Wang, L. He, Y.-S. He, Electrochem. Commun. 11 (2009) 1277.
[82] X. Li, F. Kang, X. Bai, W. Shen, Electrochem. Commun. 9 (2007) 663.
[83] B. Huang, X. Zheng, D. Jia, M. Lu, Electrochim. Acta 55 (2010) 1227.
[84] Q. Chen, J. Wang, Z. Tang, W. He, H. Shao, J. Zhang, Electrochim. Acta 52 (2007) 5251.
[85] F. Yu, J. Zhang, Y. Yang, G. Song, J. Solid State Electrochem. 14 (2010) 883.
[86] H. Huang, T. Faulkner, J. Barker, M.Y. Saidi, J. Power Sources 189 (2009) 748.
[87] M.M. Thackeray, A. de Kock, W.I.F. David, Mater. Res. Bull. 28 (1993) 1041.
[88] H.W. Chan, J.G. Duh, S.R. Sheen, J. Power Sources 115 (2003) 110.
[89] J. Molenda, M. Ziemnicki, J. Marzec, W. Zając, M. Molenda, M. Bućko, J. Power Sources 173 (2007) 707.
[90] J. Tu, X.B. Zhao, J. Xie, G.S. Cao, D.G. Zhuang, T.J. Zhu, J.P. Tu, J. Alloys Compd. 432 (2007) 313.
[91] J. Shu, T.-F. Yi, M. Shui, Y. Wang, R.-S. Zhu, X.-F. Chu, F. Huang, D. Xu, L. Hou, Comp. Mater. Sci. 50 (2010) 776.
[92] I. Taniguchi, Z. Bakenov, Powder Technol. 159 (2005) 55.
[93] X. He, J. Li, Y. Cai, Y. Wang, J. Ying, C. Jiang, C. Wan, J. Power Sources 150 (2005) 216.
[94] V. Singh, D. Joung, L. Zhai, S. Das, S.I. Khondaker, S. Seal, Prog. Mater. Sci. 56 (2011) 1178.
[95] K.S. Novoselov, Z. Jiang, Y.-H. Zhang, S.V. Morozov, H.L. Stormer, U. Zeitler, J.C. Maan, G.S. Boebinger, P. Kim, A.K. Geim, Science 315 (2007) 1379.
[96] A.K. Geim, K.S. Novoselov, Nat. Mater. 6 (2007) 183.
[97] X. Lu, M. Yu, H. Huang, R.S. Ruoff, Nanotechnology 10 (1999) 269.
[98] H. Fredriksson, D. Chakarov, B. Kasemo, Carbon 47 (2009) 1335.
[99] X.Z. Yu, C.G. Hwang, C.M. Jozwiak, A. Köhl, A.K. Schmid, A. Lanzara, J. Electron. Spectrosc. Relat. Phenom. 184 (2011) 100.

[100] C. Berger, Z. Song, X. Li, X. Wu, N. Brown, C. Naud, D. Mayou, T. Li, J. Hass, A.N. Marchenkov, E.H. Conrad, P.N. First, W.A. de Heer, Science 312 (2006) 1191.
[101] H. An, W.-J. Lee, J. Jung, Curr. Appl. Phys. 11 (2011) S81.
[102] J. Wintterlin, M.-L. Bocquet, Surf. Sci. 603 (2009) 1841.
[103] D. Li, M.B. Müller, S. Gilje, R.B. Kaner, G.G. Wallace, Nat. Nanotechnol. 3 (2008) 101.
[104] C. Gómez-Navarro, R.T. Weitz, A.M. Bittner, M. Scolari, A. Mews, M. Burghard, K. Kern, Nano Lett. 7 (2007) 3499.
[105] S. Stankovich, D.A. Dikin, R.D. Piner, K.A. Kohlhaas, A. Kleinhammes, Y. Jia, Y. Wu, S.T. Nguyen, R.S. Ruoff, Carbon 45 (2007) 1558.
[106] C. Mattevi, G. Eda, S. Agnoli, S. Miller, K.A. Mkhoyan, O. Celik, D. Mastrogiovanni, G. Granozzi, E. Garfunkel, M. Chhowalla, Adv. Funct. Mater. 19 (2009) 2577.
[107] M.J. Fernandez-Merino, L. Guardia, J.I. Paredes, S. Villar-Rodil, P. Solis-Fernandez, A. Martinez-Alonso, J.M.D. Tascon, J. Phys. Chem. C 114 (2010) 6426.
[108] S. Pei, H.-M. Cheng, Carbon 50 (2012) 3210.
[109] B.C. Brodie, Phil. Trans. R. Soc. Lond. 149 (1859) 249.
[110] W.S. Hummers, R.E. Offeman, J. Am. Chem. Soc. 80 (1958) 1339.
[111] D.R. Dreyer, S. Park, C.W. Bielawski, R.S. Ruoff, Chem. Soc. Rev. 39 (2010) 228.
[112] N.I. Kovtyukhova, P.J. Ollivier, B.R. Martin, T.E. Mallouk, S.A. Chizhik, E.V. Buzaneva, A.D. Gorchinskiy, Chem. Mater. 11 (1999) 771.
[113] D.C. Marcano, D. V Kosynkin, J.M. Berlin, A. Sinitskii, Z. Sun, A. Slesarev, L.B. Alemany, W. Lu, J.M. Tour, ACS Nano 4 (2010) 4806.
[114] F. Yang, Y. Liu, L. Gao, J. Sun, J. Phys. Chem. C 114 (2010) 22085.
[115] H. Wang, X. Wang, X. Li, H. Dai, Nano Res. 2 (2009) 336.
[116] X. Rui, J. Zhu, D. Sim, C. Xu, Y. Zeng, H.H. Hng, T.M. Lim, Q. Yan, Nanoscale 3 (2011) 4752.
[117] D. Pan, S. Wang, B. Zhao, M. Wu, H. Zhang, Y. Wang, Z. Jiao, Chem. Mater. 21 (2009) 3136.
[118] A. Lerf, H. He, M. Forster, J. Klinowski, J. Phys. Chem. B 102 (1998) 4477.
[119] H. He, J. Klinowski, M. Forster, A. Lerf, Chem. Phys. Lett. 287 (1998) 53.
[120] W. Gao, L.B. Alemany, L. Ci, P.M. Ajayan, Nat. Chem. 1 (2009) 403.
[121] W. Cai, R.D. Piner, F.J. Stadermann, S. Park, M.A. Shaibat, Y. Ishii, D. Yang, A. Velamakanni, S.J. An, M. Stoller, J. An, D. Chen, R.S. Ruoff, Science 321 (2008) 1815.
[122] T. Szabó, O. Berkesi, P. Forgó, K. Josepovits, Y. Sanakis, D. Petridis, I. Dékány, Chem. Mater. 18 (2006) 2740.
[123] H.A. Becerril, J. Mao, Z. Liu, R.M. Stoltenberg, Z. Bao, Y. Chen, ACS Nano 2 (2008) 463.
[124] H.-J. Shin, K.K. Kim, A. Benayad, S.-M. Yoon, H.K. Park, I.-S. Jung, M.H. Jin, H.-K. Jeong, J.M. Kim, J.-Y. Choi, Y.H. Lee, Adv. Funct. Mater. 19 (2009) 1987.
[125] S. Pei, J. Zhao, J. Du, W. Ren, H.-M. Cheng, Carbon 48 (2010) 4466.
[126] P. Song, X. Zhang, M. Sun, X. Cui, Y. Lin, RSC Adv. 2 (2012) 1168.
[127] G. Williams, B. Seger, P.V. Kamat, ACS Nano 2 (2008) 1487.
[128] M. Zhou, Y. Wang, Y. Zhai, J. Zhai, W. Ren, F. Wang, S. Dong, Chem. Eur. J. 15 (2009) 6116.
[129] D. Wei, L. Grande, V. Chundi, R. White, C. Bower, P. Andrew, T. Ryhänen, Chem. Commun. 48 (2012) 1239.
[130] H.C. Schniepp, J.-L. Li, M.J. McAllister, H. Sai, M. Herrera-Alonso, D.H. Adamson, R.K. Prud'homme, R. Car, D.A. Saville, I.A. Aksay, J. Phys. Chem. B 110 (2006) 8535.
[131] X. Wang, L. Zhi, K. Müllen, Nano Lett. 8 (2008) 323.
[132] D. Yang, A. Velamakanni, G. Bozoklu, S. Park, M. Stoller, R.D. Piner, S. Stankovich, I. Jung, D.A. Field, C.A. Ventrice, R.S. Ruoff, Carbon 47 (2009) 145.
[133] M.J. McAllister, J.-L. Li, D.H. Adamson, H.C. Schniepp, A.A. Abdala, J. Liu, M. Herrera-Alonso, D.L. Milius, R. Car, R.K. Prud'homme, I.A. Aksay, Chem. Mater. 19 (2007) 4396.
[134] R. Span, W. Wagner, J. Phys. Chem. Ref. Data 25 (1996) 1509.
[135] S.H. Huh, in: S. Mikhailov (Ed.), Physics and Applications of Graphene – Experiments (2011), pp. 73–90.
[136] B.J. Schultz, C.J. Patridge, V. Lee, C. Jaye, P.S. Lysaght, C. Smith, J. Barnett, D.A. Fischer, D. Prendergast, S. Banerjee, Nat. Commun. 2 (2011) 372.
[137] J. Zhao, S. Pei, W. Ren, L. Gao, H.-M. Cheng, ACS Nano 4 (2010) 5245.
[138] Z.L. Wang, D. Xu, Y. Huang, Z. Wu, L.M. Wang, X.B. Zhang, Chem. Commun. 48 (2012) 976.
[139] I. Jung, D.A. Dikin, R.D. Piner, R.S. Ruoff, Nano Lett. 8 (2008) 4283.
[140] X. Gao, J. Jang, S. Nagase, J. Phys. Chem. C 114 (2010) 832.
[141] Y. Xu, H. Bai, G. Lu, C. Li, G. Shi, J. Am. Chem. Soc. 130 (2008) 5856.
[142] W. Lv, D.-M. Tang, Y.-B. He, C.-H. You, Z.-Q. Shi, X.-C. Chen, C.-M. Chen, P.-X. Hou, C. Liu, Q.-H. Yang, ACS Nano 3 (2009) 3730.
[143] J.I. Paredes, S. Villar-Rodil, A. Martínez-Alonso, J.M.D. Tascón, Langmuir 24 (2008) 10560.
[144] S. Brunauer, P.H. Emmett, E. Teller, J. Am. Chem. Soc. 60 (1938) 309.
[145] Z. Luo, T. Yu, J. Shang, Y. Wang, S. Lim, L. Liu, G.G. Gurzadyan, Z. Shen, J. Lin, Adv. Funct. Mater. 21 (2011) 911.
[146] M.M. Doeff, J.D. Wilcox, R. Kostecki, G. Lau, J. Power Sources 163 (2006) 180.
[147] A.C. Ferrari, J.C. Meyer, V. Scardaci, C. Casiraghi, M. Lazzeri, F. Mauri, S. Piscanec, D. Jiang, K.S. Novoselov, S. Roth, A.K. Geim, Phys. Rev. Lett. 97 (2006) 187401.
[148] W. Guoping, Z. Qingtang, Y. Zuolong, Q. Meizheng, Solid State Ionics 179 (2008) 263.
[149] X. Wang, S. Chen, in: S. Mikhailov (Ed.), Physics and Applications of Graphene – Experiments (2011), pp. 136–168.
[150] Z.-S. Wu, D.-W. Wang, W. Ren, J. Zhao, G. Zhou, F. Li, H.-M. Cheng, Adv. Funct. Mater. 20 (2010) 3595.
[151] L. Kavan, R. Bacsa, M. Tunckol, P. Serp, S.M. Zakeeruddin, F. Le Formal, M. Zukalova, M. Graetzel, J. Power Sources 195 (2010) 5360.
[152] A. Varzi, C. Täubert, M. Wohlfahrt-Mehrens, Electrochim. Acta 78 (2012) 17.
[153] B. Jin, E.M. Jin, K.-H. Park, H.-B. Gu, Electrochem. Commun. 10 (2008) 1537.
[154] W.-M. Chen, L. Qie, L.-X. Yuan, S.-A. Xia, X.-L. Hu, W.-X. Zhang, Y.-H. Huang, Electrochim. Acta 56 (2011) 2689.
[155] H.C. Shin, W.I. Cho, H. Jang, Electrochim. Acta 52 (2006) 1472.
[156] O. Toprakci, H.A.K. Toprakci, L. Ji, G. Xu, Z. Lin, X. Zhang, ACS Appl. Mater. Interfaces 4 (2012) 1273.
[157] D.-H. Kim, J. Kim, Electrochem. Solid-State Lett. 9 (2006) A439.
[158] M. Takahashi, H. Ohtsuka, K. Akuto, Y. Sakurai, J. Electrochem. Soc. 152 (2005) A899.
[159] C. Zhu, Y. Yu, L. Gu, K. Weichert, J. Maier, Angew. Chem. Int. Ed. 50 (2011) 6278.
[160] A.S. Aricò, P. Bruce, B. Scrosati, J.-M. Tarascon, W. Van Schalkwijk, Nat. Mater. 4 (2005) 366.
[161] P.G. Bruce, B. Scrosati, J.-M. Tarascon, Angew. Chem. Int. Ed. 47 (2008) 2930.
[162] A.Y. Shenouda, H.K. Liu, J. Alloys Compd. 477 (2009) 498.
[163] Z.J. Wu, H.F. Yue, L.S. Li, B.F. Jiang, X.R. Wu, P. Wang, J. Power Sources 195 (2010) 2888.
[164] R. Amin, C. Lin, J. Peng, K. Weichert, T. Acartürk, U. Starke, J. Maier, Adv. Funct. Mater. 19 (2009) 1697.
[165] R. Dominko, M. Gaberscek, J. Drofenik, M. Bele, S. Pejovnik, J. Jamnik, J. Power Sources 119–121 (2003) 770.
[166] Q. Chen, X. Qiao, C. Peng, T. Zhang, Y. Wang, X. Wang, Electrochim. Acta 78 (2012) 40.
[167] S.-C. Yin, H. Grondey, P. Strobel, M. Anne, L.F. Nazar, J. Am. Chem. Soc. 125 (2003) 10402.
[168] S. Patoux, C. Wurm, M. Morcrette, G. Rousse, C. Masquelier, J. Power Sources 119–121 (2003) 278.
[169] L. Wang, X. Zhou, Y. Guo, J. Power Sources 195 (2010) 2844.
[170] Y.Q. Qiao, J.P. Tu, X.L. Wang, D. Zhang, J.Y. Xiang, Y.J. Mai, C.D. Gu, J. Power Sources 196 (2011) 7715.
[171] Y. Zhang, Q. Huo, Y. Lv, L. Wang, A. Zhang, Y. Song, G. Li, H. Gao, T. Xia, H. Dong, J. Alloys Compd. 542 (2012) 187.
[172] K. Nagamine, T. Honma, T. Komatsu, J. Power Sources 196 (2011) 9618.
[173] X.H. Rui, C. Li, C.H. Chen, Electrochim. Acta 54 (2009) 3374.
[174] H. Wang, Y. Li, C. Huang, Y. Zhong, S. Liu, J. Power Sources 208 (2012) 282.
[175] L. Zhang, H. Xiang, Z. Li, H. Wang, J. Power Sources 203 (2012) 121.
[176] Y.Q. Qiao, J.P. Tu, Y.J. Mai, L.J. Cheng, X.L. Wang, C.D. Gu, J. Alloys Compd. 509 (2011) 7181.
[177] Z. Bakenov, I. Taniguchi, J. Power Sources 195 (2010) 7445.
[178] L. Damen, F. De Giorgio, S. Monaco, F. Veronesi, M. Mastragostino, J. Power Sources 218 (2012) 250.
[179] D. Wang, H. Buqa, M. Crouzet, G. Deghenghi, T. Drezen, I. Exnar, N.-H. Kwon, J.H. Miners, L. Poletto, M. Grätzel, J. Power Sources 189 (2009) 624.
[180] J. Kim, Y.-U. Park, D.-H. Seo, J. Kim, S.-W. Kim, K. Kang, J. Electrochem. Soc. 158 (2011) A250.
[181] M.M. Thackeray, W.I.F. David, P.G. Bruce, J.B. Goodenough, Mater. Res. Bull. 18 (1983) 461.
[182] L. Lu, X. Han, J. Li, J. Hua, M. Ouyang, J. Power Sources 226 (2013) 272.
[183] G. Amatucci, J.-M. Tarascon, J. Electrochem. Soc. 149 (2002) K31.
[184] D. Aurbach, M.D. Levi, K. Gamulski, B. Markovsky, G. Salitra, E. Levi, U. Heider, L. Heider, R. Oesten, J. Power Sources 81–82 (1999) 472.
[185] Y. Xia, Y. Zhou, M. Yoshio, J. Electrochem. Soc. 144 (1997) 2593.
[186] A. Blyr, C. Sigala, G. Amatucci, D. Guyomard, Y. Chabre, J.-M. Tarascon, J. Electrochem. Soc. 145 (1998) 194.
[187] D. Arumugam, G. Paruthimal Kalaignan, J. Electroanal. Chem. 624 (2008) 197.
[188] C. Qing, Y. Bai, J. Yang, W. Zhang, Electrochim. Acta 56 (2011) 6612.
[189] Y. Chen, K. Xie, Y. Pan, C. Zheng, J. Power Sources 196 (2011) 6493.
[190] H. Xia, K.R. Ragavendran, J. Xie, L. Lu, J. Power Sources 212 (2012) 28.
[191] W. Tang, X.J. Wang, Y.Y. Hou, L.L. Li, H. Sun, Y.S. Zhu, Y. Bai, Y.P. Wu, K. Zhu, T. van Ree, J. Power Sources 198 (2012) 308.